Finite-time extended state observer and fractional-order sliding mode controller for impulsive hybrid port-Hamiltonian systems with input delay and actuators saturation: Application to ball-juggler robots

Yousef Farid[a], Fabio Ruggiero[a]

[a] *PRISMA Lab, Department of Electrical Engineering and Information Technology, University of Naples Federico II, Via Claudio 21, 80125, Naples, Italy*

Abstract

This paper addresses the robust control problem of mechanical systems with hybrid dynamics in port-Hamiltonian form. It is assumed that only the position states are measurable, and time-delay and saturation constraint affect the control signal. An extended state observer is designed after a coordinate transformation. The effect of the time delay in the control signal is neutralized by applying Padé approximant and augmenting the system states. An assistant system with faster convergence is developed to handle actuators saturation. Fractional-order sliding mode controller acts as a centralized controller and compensates for the undesired effects of unknown external disturbance and parameter uncertainties using the observer estimation results. Stability analysis shows that the closed-loop system states, such as the observer tracking error, and the position/velocity tracking errors, are finite-time stable. Simulation studies on a two ball-playing juggler robot with three degrees of freedom validate the theoretical results' effectiveness.

Keywords: Impulsive hybrid systems, Port-Hamiltonian dynamics, Extended state observer, Fractional sliding surface, Finite-time control, Input delay

1. Introduction

The port-controlled Hamiltonian (pH) formulation is a powerful tool for modeling electrical and mechanical systems, as well as most of the dynamical systems [1]. In the last years, outstanding outcomes have been reported on control and stability analysis of pH systems [2, 3, 4]. Most of the presented results consider the systems to work on one operation mode. In contrast, in many situations, interaction conditions impose hybrid features on system dynamics (i.e., instantaneous jumps in some system states' values caused by impacts or similar). On the other hand, measurement problems of high order states, actuator nonlinearities, and undesired effects of lumped uncertainties and external disturbances are challenges that the designed control system must cope with. Besides, in interactive hybrid systems, the convergence speed or transient state response within a fixed time is essential. We propose an observer-based finite-time robust control algorithm for hybrid dynamical systems in pH form to tackle these problems, which preserve the closed-loop control system's stability against instantaneous changes in the state values and actuator constraints.

1.1. Related works

Hybrid systems with parameters or state jumps, or varying environmental properties, belong to the class of dynamical systems described by one(multiple) continuous-time behavior(s) with state interruption in some switching instants [5, 6, 7]. These systems are successful in representing the intricate and latent features of real systems occurring in engineering applications [8, 9]. Many works have been reported in the literature on the stability of hybrid systems [10, 11]. Common Lyapunov functions (CLFs) and multiple Lyapunov functions (MLFs) are usually employed as powerful tools to investigate the stabilization problem of hybrid systems [12]. Average dwell time (ADT) is

Email addresses: yousef.farid@unina.it (Yousef Farid), fabio.ruggiero@unina.it (Fabio Ruggiero)

another useful technique [13]. H_∞-based robust controller design was addressed in [14] along with an ADT method for the stability analysis.

As well known, the dynamic equations of most of the electro-mechanical processes such as electric vehicles, unmanned aerial vehicles, and surgery robotic systems belong to the particular class of pH dynamical systems [15, 16, 17]. In a pH system, the Hamiltonian function, which is the sum of kinetic and potential energies, can be labeled as a Lyapunov function candidate in the stability analysis. In the last decade, pH-based modeling and control have attracted much attention and have provided significant outcomes [18, 19, 20]. In practical applications, it is common the possibility to measure the position states only: the velocity states are often not measurable or noisy. On the other hand, other terms that affect the system dynamics, such as parameter uncertainty and external disturbances, may not be measurable. In this direction, a full-order state observer for a general class of pH systems with exponential stability property was proposed in [21]. In that work, the effects of parameter uncertainties and external disturbance were not considered. By developing a composite control plan and based on a nonlinear disturbance estimator, pH systems' stabilization problem was studied in [22], where the proposed control scheme assumes that all the system states are measurable. Recently, a work about the stabilization problem and H_∞ control of a hybrid pH system with unstable mode and actuator saturation has been published [23].

An appealing mechanical system falling within the category of pH hybrid systems is the ball juggling robot. Juggling is based on the repetitively coordinated execution of the batting nonprehensile motion primitive [24], which combines catching and throwing in a single collision instant [25]. Juggling tasks can be thus considered part of cooperative nonprehensile manipulation action in which the dynamics of the manipulated objects and the skillful function of the jugglers are taken into account [26, 25, 27, 28, 29]. Juggling actions are challenging for humans because they need high concentration, rapid reaction, dexterity, and high adaptability to the environment. Besides, the juggled object is repetitively caught and thrown, thus creating and breaking contacts with the manipulator iteratively. Therefore, from the viewpoint of dynamic modeling of the juggler robots, the juggler's equations can be described by a hybrid/switching dynamics. In robotic juggler systems, usually, more control energy is needed due to the jugglers' high-speed motion, the existence of impact effects, parameter uncertainties, and external disturbances. This may cause saturation of the actuators. Neglecting of the actuator saturation problem may leads to the performance degradation or even instability of the closed-loop system [30]. Moreover, factors such as the computation time, the communication channel, the sampling time, and the sensor measurements may lead to input delays in the control signal. The interaction between the delayed control signal and the system's switching property may deteriorate the performance or even lead to instability. A composite control design for a class of hybrid impulsive systems with time-delay in the states, actuator saturation, and matched/mismatched disturbances was studied in [31]. In [32], finite-time optimal control design for a class of double integrator system under input delay and actuator saturation has been investigated.

Finite-time stability analysis is a criterion that can be used for evaluating the stability characteristics in dynamical systems. Newly, the finite-time control problem for stabilizing hybrid systems with input-delay and actuator saturation has been investigated [33], where the addressed system is linear and not robust against parameter uncertainties and external disturbances. Using fractional-operators in design procedure can significantly improve the transient and steady-state performance, reinforce the robustness, and reduce/suppress the chattering phenomena [34, 35]. Therefore, fractional calculus was used to control singularly perturbed systems [36], solve optimal control problems [37], control legged robots [38], carry out fault diagnosis and classification [39], and address formation control of multi-agent systems [40].

1.2. Contributions

Despite exemplary achievements in the control and stabilization of hybrid systems, several issues still need to be discussed, such as state observer design in practical applications, disturbance reconstruction, finite-time convergence problem, and constraints and delays in the control signal, simultaneously. Therefore, in this study, a finite-time robust control algorithm, based on a fractional-order controller, is proposed for hybrid pH systems, which preserves the closed-loop stability against interaction impacts and actuators saturation.

The key contributions of this research work are summarized in the following. *i)* An extended state observer is proposed to estimate velocities state and lumped disturbances in a finite-time. *ii)* Using Padé approximation, an auxiliary system is designed. A new variable is added to the main system, eliminating the time delay of the control signal from the calculations. *iii)* To deal with actuator saturation, another assistant system with finite-time convergence property is introduced. *iv)* A finite-time fractional-order sliding surface is defined. Based on fractional calculus, a

robust centralized controller is designed. *v)* The robustness against unknown parameter uncertainty and external disturbance is fulfilled by accommodating the central controller with the estimated results. *vi)* Lyapunov stability theorem ensures the finite-time stability of the close loop system.

To bolster the contributions mentioned above, the trajectory tracking and the robustness performance of two juggler robots in a ball-playing scenario, under parameter uncertainty and external disturbance, are evaluated in some simulation case studies.

1.3. Outline

The remaining of this paper is organized as follows. The hybrid dynamic description of the Lagrangian systems and some preliminaries are exhibited in Section 2. The main results on the extended-stated observer design, the robust fractional-order sliding mode controller, and the stability analysis of the closed-loop system are presented in Section 3. In Section 4, numerical simulations are provided to test the effectiveness of the theoretical results. The conclusion is brought in Section 5.

2. Problem statement and some preliminaries

In this section, some preliminary knowledge of mechanical processes with hybrid dynamics in the pH form and the fractional calculus are introduced.

2.1. Modelling of hybrid mechanical processes in pH form

Without loss of generality, in order to develop the mathematical modelling part, it is supposed that an impact causes the instantaneous jump in some system state values. Hence, two phases can be recognzied: a free-motion or impact-less phase and an impact phase. Using Euler-Lagrange formulation, taking into account both time delay in the control signal and saturation constraints, the impulsive hybrid equations of a mechanical system can be written as

$$\begin{cases} M(q)\ddot{q} + C(q,\dot{q})\dot{q} + g_0(q) + \delta(q,\dot{q}) = B\text{sat}(\tau(t-t_d)) + \tau_d, & \vartheta(q,\dot{q}) \neq 0 \\ q^+ = \Delta_n(q)q^-, & \vartheta(q,\dot{q}) = 0 \\ \dot{q}^+ = \Delta_s(q,\dot{q})\dot{q}^-, & \vartheta(q,\dot{q}) = 0 \end{cases} \tag{1}$$

where $q \in \mathbb{R}^n$ represents the state and $\dot{q} \in \mathbb{R}^n$ its time derivative; $M(q) \in \mathbb{R}^{n\times n}$, $C(q,\dot{q}) \in \mathbb{R}^{n\times n}$, and $g_0(q) \in \mathbb{R}^n$ are called the inertia matrix, the Coriolis matrix, and the vector of gravitational terms, respectively. Also, $B \in \mathbb{R}^{n\times m}$ is the allocation matrix for the actuation $\tau \in \mathbb{R}^m$, with $0 < m \leq n$, while $t_d \in \mathbb{R}$ is the related time delay. The saturation function $\text{sat}(\tau) = \left[\text{sat}(\tau_1)\cdots\text{sat}(\tau_m)\right]^T$ is defined as

$$\text{sat}(\tau_i) = \begin{cases} \tau_{max} & \tau_i \geq \tau_{max}, \\ \tau_{min} & \tau_i \leq \tau_{min}, \\ \tau_i & \text{otherwise}, \end{cases}$$

where $\tau_i \in \mathbb{R}$ is the i-th component of τ, with $i = 1,\ldots,m$, and $\tau_{max}, \tau_{min} \in \mathbb{R}$ are the maximum and minimum allowed values of the i-th input component, respectively. The function $\delta(q,\dot{q}) \in \mathbb{R}^n$ contains all uncertainty and damping terms of the system, while $\tau_d \in \mathbb{R}^n$ represents the external disturbance vector. Besides, $\vartheta(q,\dot{q}) = 0$ is a state-dependent impact condition, the apexes + and − denote the quantities at a time instant after and before the impact, respectively, and $\Delta_n, \Delta_s(q,\dot{q}) \in \mathbb{R}^{n\times n}$ are the position renaming and the velocity resetting matrices, respectively.

Remark 1. *It is important to note that most of the robotic systems subjected to the impacts, such as biped robots and impact mechanical oscillatorsm can be modelled by the impulsive hybrid nonlinear dynamics described in* (1) *[41, 42, 43]. This impulsive hybrid system combines two different dynamics: a continuous-time one, which defines its flux if $\vartheta(q,\dot{q})$ has nonzero value (we call those continuous subsystems modes); discrete-time dynamics, which describes the state jumps if $\vartheta(q,\dot{q})$ takes a zero value (those are the discrete modes of system). The variable $\vartheta(q,\dot{q})$ orchestrates the transition between continuous and discrete modes.*

Consider the Lagrangian function of the system (1) as

$$L(q,\dot{q}) = \frac{1}{2}\dot{q}^T M(q)\dot{q} - V(q), \tag{2}$$

where $V(q) \in \mathbb{R}$ is the potential energy of (1). Defining the momentum vector of the system as $p = \dfrac{\partial L}{\partial \dot{q}} = M(q)\dot{q} \in \mathbb{R}^n$, the dynamic equations (1) in impact-less times $t \neq t_k$ can be rewritten as

$$\begin{cases} \dot{q} = M^{-1}(q)p, \\ \dot{p} = \dot{M}(q)\dot{q} - C(q,\dot{q})\dot{q} - g_0(q) + B\text{sat}(\tau(t-t_d)) + \tau_d - \delta(q,\dot{q}), \end{cases} \tag{3}$$

The Hamiltonian function of (3) is defined by [44, p. 165]

$$H(q,p) = p^T\dot{q} - L(q,p), \tag{4}$$

where it is worth recalling that $\dot{q} = M(q)^{-1}p$ and then $L(q,p) = \dfrac{1}{2}p^T M(q)^{-1}p - V(q)$. The partial derivative of the Hamiltonian with respect to p is calculated as [44, p. 167]

$$\nabla_p H = \frac{\partial H}{\partial p} = \dot{q} = M(q)^{-1}p, \tag{5}$$

while its partial derivate with respect to q is calculated as [44, p. 165]

$$\nabla_q H = \frac{\partial L(q,\dot{q})}{\partial q}. \tag{6}$$

Recalling the Euler-Lagrange equation

$$\frac{d}{dt}\Big(\frac{\partial L(q,\dot{q})}{\partial \dot{q}}\Big) - \frac{\partial L(q,\dot{q})}{\partial q} = B\tau, \tag{7}$$

it yields

$$\frac{\partial L}{\partial q} = \dot{p} - B\tau. \tag{8}$$

Folding (8) into (6), yields

$$\nabla_q H = \frac{\partial L(q,\dot{q})}{\partial q} = -\dot{p} + B\tau \tag{9}$$

From (3), (5), (9), and considering saturation constraint, parameter uncertainty and external disturbance terms, it is evident that $\nabla_p H = M^{-1}(q)p$, $\nabla_q H = C(q,\dot{q})\dot{q} + g_0(q) - \dot{M}(q)\dot{q}$.

Therefore, the general pH form of (1) can be expressed as

$$\begin{cases} \dot{x} = \Omega\nabla H + G\text{sat}\left(\tau(t-t_d)\right) + d(x,t), & \vartheta(x) \neq 0, \\ x^+ = \Delta_p(x), & \vartheta(x) = 0, \end{cases} \tag{10}$$

with $x = \begin{bmatrix} x_1^T & x_2^T \end{bmatrix}^T = \begin{bmatrix} q^T & p^T \end{bmatrix}^T$, $\nabla H = \begin{bmatrix} \left(\nabla_q H\right)^T & \left(\nabla_p H\right)^T \end{bmatrix}^T$, $G = \begin{bmatrix} O_{m\times n} & B^T \end{bmatrix}^T$, $d(x,t) = \begin{bmatrix} 0_n{}^T & (\tau_d - \delta(q,\dot{q}))^T \end{bmatrix}^T$, and $\Delta_p(x) = \begin{bmatrix} (\Delta_n q^-)^T & \delta_p(x,\Delta_s)^T \end{bmatrix}^T$ in which the vector $\delta_p(x,\Delta_s)$ addresses the impact at the momenta's level, that is $\delta_p(x,\Delta_s) = p^+ = M(q^+)\dot{q}^+ = M(\Delta_n q^-)\Delta_s\dot{q}^- = M(\Delta_n q^-)\Delta_s M^{-1}(q^-)p^-$, and

$$\Omega = \begin{bmatrix} O_{n\times n} & I_n \\ -I_n & O_{n\times n} \end{bmatrix},$$

where $I_n \in \mathbb{R}^{n\times n}$ and $O_{i\times j} \in \mathbb{R}^{i\times j}$ are identity and zero matrices of proper dimensions, respectively, and $0_n \in \mathbb{R}^n$ is the zero vector.

Theorem 1. *For a nonlinear system $\dot{x} = -\Sigma\nabla H(x)$, where $\Sigma \in \mathbb{R}^{2n\times 2n}$ is a positive definite matrix, if the energy function $H(x)$ is designed as*

$$H(x) = (x^T Y x)^\beta, \tag{11}$$

where $1 < \beta < 2$, and $Y \in \mathbb{R}^{2n\times 2n}$ is a positive definite matrix, then the system is finite-time stable.

Proof. See [45, Theorem 1]. □

Remark 2. *The value of β in* (11) *determines the type of stability (i.e., finite-time or asymptotic stability). In particular, if $\beta \geq 2$ then the selected Hamiltonian function* (11) *cannot guarantee the finite-time stability, and the obtained results decline to the traditional asymptotic stability [46].*

Definition 1 ([47])**.** *The hybrid system* (10)*, with $\tau = 0$ and $d(x,t) = 0$, under the condition $H(x(t_0)) < b_1 \Rightarrow H(x(t)) < b_2,\ \forall t \in (0, T_f]$, where $0 < b_1 < b_2$ and $T_f > 0$, is finite-time stable.*

Lemma 1 ([38])**.** *For a nonlinear system $\dot{x} = f(x(t), t)$, if the relation between the Lyapunov function $V(x(t))$ and its time derivative is*

$$\dot{V}(x(t)) = -aV(x(t)) - bV^c(x(t)), \tag{12}$$

where $a > 0$, $b > 0$, and $0 < c < 1$, then the state trajectories will converge to the equilibrium point $x(t) = 0$ in a finite time $t_r \in \mathbb{R}$ characterized by

$$t_r \leq t_0 + \frac{1}{a(1-c)} \ln\left(\frac{aV^{1-c}(x(t_0)) + b}{b}\right) \tag{13}$$

where $\ln(\cdot)$ is the natural logarithmic function, and $t_0 \in \mathbb{R}$ is the initial time.

Remark 3. *For any scalar function $\mathcal{F}_i = (x^T \Upsilon_i x)^\beta > 0$, where $\Upsilon_i \in \mathbb{R}^{2n\times 2n}$ is a diagonal positive definite matrix and $1 < \beta < 2$, if $\Upsilon_i \leq \varrho^{\frac{1}{\beta}} \Upsilon_j$ holds element-wise for each diagonal component, with $\varrho > 1$ and $i \neq j$, then $\mathcal{F}_i \leq \varrho \mathcal{F}_j$.*

2.2. Fractional calculus

To contextualize this work, the fundamental definition and properties of fractional calculus follow.

Among the fractional operators, Caputo and Riemann–Liouville ones are often employed within the field of control systems [40]. Since the Caputo fractional derivative has well-accepted physical interpretations [48], the related fractional operator is here employed. The Caputo fractional derivative of order $\alpha \geq 0$ is defined as

$$D^\alpha f(t) = \frac{1}{\Gamma(n-\alpha)} \int_{t_0}^{t} \frac{f^n(r)}{(t-r)^{\alpha-n+1}} \mathrm{d}r, \tag{14}$$

where $f(t) \in \mathbb{R}^n$ is a time-dependent function, $t_0 \in \mathbb{R}$ is the initial integration time, $m - 1 < \alpha < m$, $m \geq 1$, and Γ is the so-called *Gamma function*

$$\Gamma(z) = \int_0^\infty \iota^{z-1} e^{-\iota} \mathrm{d}\iota. \tag{15}$$

Property 1 ([48])**.** *For the optional scalars $a_1, a_2 \in \mathbb{R}$, the fractional orders $\alpha_1, \alpha_2 \geq 0$, and two time-dependent functions $f_1(t), f_2(t) \in \mathbb{R}$, the following relations hold*

$$D^\alpha(a_1 f_1(t) + a_2 f_2(t)) = a_1 D^\alpha f_1(t) + a_2 D^\alpha f_2(t), \tag{16}$$

$$D^{1-\alpha}(D^\alpha f(t)) = \dot{f}(t), \tag{17}$$

and

$$D^{\alpha_1}(D^{\alpha_2} f(t)) = D^{\alpha_1+\alpha_2} f(t). \tag{18}$$

2.3. Problem statement

This study aims to design a robust control law for the impulsive hybrid pH system (10), leading the measured states to the desired ones. The joint velocities are not measurable. An extended state observer-based robust fractional-order sliding mode controller is proposed. The controller structure ensures that the closed-loop system signals are finite-time stable in both impact-less and impact phases.

Remark 4. *Notice that our previous work [45] requires both position information and velocity information. Here, the devised control law requires position information only. Also, differently from [45], actuator saturation is here considered explicitly. Besides, this work also introduces (unknown) time delay in the control action. Finally, the proposed extended-state observer estimates the system states and the unknown function simultaneously.*

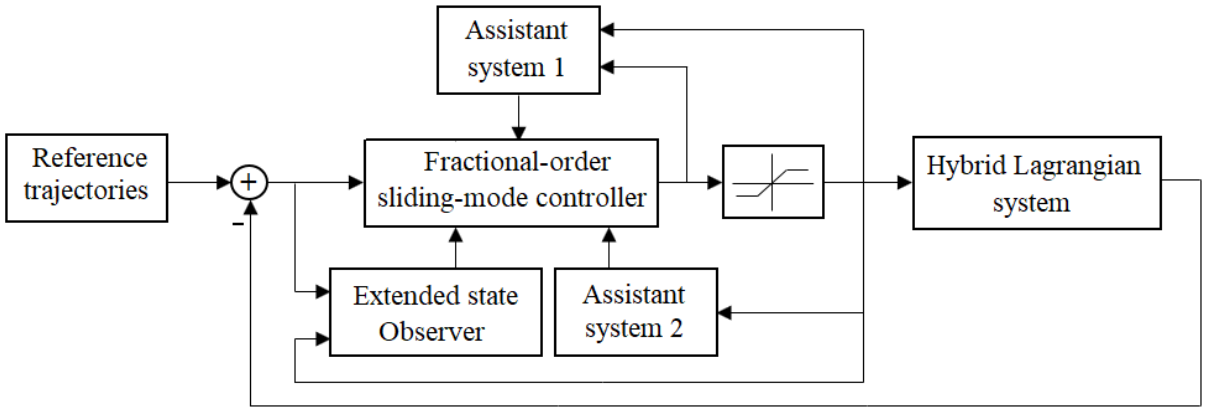

Figure 1: The proposed observer-based robust control scheme for hybrid mechanical system.

3. Main theoretical results

The proposed control scheme is shown in Fig. 1. The main focus is put on the finite-time extended state, the disturbance observer design, and the centralized robust fractional-order sliding-mode controller. Assistant systems cope with saturation and input time-delay. In the following, the design of these blocks are explained. Firstly, the state observer and the robust controller are designed without considering impact conditions. These are then considered for the stability of the closed-loop system.

In the following, Υ_i, with $i = \{o, s, c\}$, are diagonal matrix of appropriate dimension, in which the entries are positive time-decreasing functions. Explicit dependency on time is dropped for simplicity.

3.1. Finite-time extended-state observer design

In this section, the design procedure for the extended state observer is explained.

Adding and subtracting the term $K_x x$ to the continuous part of the impulsive hybrid pH system (10) yields

$$\dot{x} = -K_x x + \phi(x) + G\text{sat}(\tau(t - t_d)) + d(x, t), \tag{19}$$

where $K_x \in R^{2n\times 2n}$ is a positive definite matrix and $\phi(x) = \Omega\nabla H(x) + K_x x \in \mathbb{R}^{2n}$. Defining a new state variable $w = d(x, t) \in \mathbb{R}^{2n}$, the extended state form of the system (19) becomes

$$\begin{cases} \dot{x} = -K_x x + \phi(x) + G\text{sat}(\tau(t - t_d)) + w, \\ \dot{w} = \theta, \\ y = L_0 x, \end{cases} \tag{20}$$

where $\theta \in R^{2n}$ is the time derivative of $d(x,t)$, $y \in R^n$ is the output vector of the system and includes the measurable states, and $L_0 = \begin{bmatrix} I_n & O_{n\times n} \end{bmatrix} \in \mathbb{R}^{n\times 2n}$ is the output matrix. Consider the following coordinates transformation

$$\begin{bmatrix} x \\ w \end{bmatrix} = \begin{bmatrix} I_{2n} & O_{2n\times 2n} \\ \Lambda & I_{2n} \end{bmatrix} \begin{bmatrix} z_1 \\ z_2 \end{bmatrix}, \tag{21}$$

where $z_1 \in R^{2n}$ and $z_2 \in R^{2n}$ are new state vectors and $\Lambda \in R^{2n\times 2n}$ is a positive definite matrix. By applying (21) to (20), the new form of the extended state hybrid pH system in the z-coordinates is obtained as

$$\begin{cases} \dot{z} = Az + \Phi(z) + \mathcal{G}\text{sat}\left(\tau_z(t - t_d)\right) + \bar{\theta}, \\ y = Lz, \end{cases} \tag{22}$$

where $z = \begin{bmatrix} z_1^T & z_2^T \end{bmatrix}^T$, $\Phi(z) = \begin{bmatrix} \phi(x)^T & -\Lambda\phi(x)^T \end{bmatrix}^T$, $\mathcal{G} = \text{diag}(G, -\Lambda G)$, $L = \begin{bmatrix} L_0 & O_{n\times 2n} \end{bmatrix}$, $\bar{\theta} = \begin{bmatrix} O_{2n}^T & \theta^T \end{bmatrix}^T$, $\tau_z = \begin{bmatrix} \tau^T & \tau^T \end{bmatrix}^T$, and $A = \begin{pmatrix} \Lambda - K_x & I_{2n} \\ -\Lambda(\Lambda - K_x) & -\Lambda \end{pmatrix}$.

The proposed finite time extended state and disturbance observer has the following structure

$$\begin{cases} \dot{\hat{z}} = A\hat{z} + \Phi(\hat{z}) + \mathcal{G}\text{sat}\left(\tau_z(t - t_d)\right) - L_{o_1}\tilde{y}^{\sigma} - L_{o_2}\tanh\left(\tilde{y}/\rho\right), \\ \hat{y} = L\hat{z}, \end{cases} \tag{23}$$

where $\hat{z} \in \mathbb{R}^{4n}$ is the estimated value of z, $\hat{y} \in \mathbb{R}^n$ is the estimated value of y, $\tilde{y} = \hat{y} - y \in \mathbb{R}^n$ is the output estimation error, $L_{o_1} \in R^{4n\times n}$ and $L_{o_2} \in R^{4n\times n}$ are the observer gain matrices, $0 < \sigma < 1$, and $\rho > 0$ determines the shape of the $\tanh(\cdot)$ function.

Defining the observer error vector as $\tilde{z} = \hat{z} - z$, its time derivative along the trajectories of (22) and (23) yields

$$\begin{cases} \dot{\tilde{z}} = A\tilde{z} + \Phi(\hat{z}) - \Phi(z) - L_{o_1}\tilde{y}^{\sigma} - L_{o_2}\tanh\left(\tilde{y}/\rho\right) - \bar{\theta}, \\ \tilde{y} = L\tilde{z}. \end{cases} \tag{24}$$

Assumption 1. *The disturbance function changes continuously and without any disruption over time. This means that the norm of $\bar{\theta}$ is bounded, $\|\bar{\theta}\| \leq l_\theta$, where $l_\theta > 0$.*

Assumption 2. *For two state variables z and $\hat{z}$, and $\gamma > 0$, the following Lipchitz condition holds $\|\Phi(\hat{z}) - \Phi(z)\| \leq \gamma\|\hat{z} - z\|$.*

Theorem 2. *Consider the dynamic equation of the extended state and disturbance observer tracking error* (24)*. Under the Assumptions 1 and 2, if the positive definite matrix Q satisfies the following Lyapunov equation*

$$A^T\Upsilon_o + \Upsilon_o A = -Q, \tag{25}$$

where $\Upsilon_o \in R^{4n\times 4n}$, and if $\|L_{o_2}\| \geq l_\theta$, then the estimation error of the extended state $\tilde{z}$ will converge to the origin through the following finite reaching time

$$t_r \leq t_0 + \frac{1}{(\lambda_{min}(Q\Upsilon_o^{-1}) - 2\gamma)(1-\sigma)} \ln\left(\frac{(\lambda_{min}(Q\Upsilon_o^{-1}) - 2\gamma)V_o^{\frac{1-\sigma}{\beta}} + 2\lambda_{min}(L_{o_1}L^{\sigma})}{2\lambda_{min}(L_{o_1}L^{\sigma})} \right), \tag{26}$$

where $\gamma > 0$, $V_o(\cdot)$ is the energy function of (24) *and t_0 is the initial time instant.*

Proof. Let the Lyapunov function be

$$V_o(\tilde{z}(t)) = H_o(\tilde{z}(t)) = \left(\tilde{z}^T\Upsilon_o\tilde{z}\right)^{\beta}. \tag{27}$$

Taking the time derivative of (27) along the dynamic of the observer tracking error (24) gives

$$\dot{V}_o(\tilde{z}(t)) = 2\beta\Big(\tilde{z}^T\Upsilon_o\tilde{z}\Big)^{\beta-1}\Big[\frac{1}{2}\tilde{z}^T(A^T\Upsilon_o + \Upsilon_o A)\tilde{z} + \tilde{z}^T\Upsilon_o\left(\Phi(\hat{z}) - \Phi(z)\right) - \tilde{z}^T\Upsilon_o L_{o_1}(L\tilde{z})^{\sigma} - \tilde{z}^T\Upsilon_o L_{o_2}\tanh\left(L\tilde{z}/\rho\right) - \tilde{z}^T\Upsilon_o\bar{\theta}\Big]. \tag{28}$$

Folding (25) into (28) and distributing $2\beta\Big(\tilde{z}^T\Upsilon_o\tilde{z}\Big)^{\beta-1}$ on the right side of (28) yield

$$\begin{aligned}\dot{V}_o(\tilde{z}(t)) \leq & -\beta\Big(\tilde{z}^T\Upsilon_o\tilde{z}\Big)^{\beta-1}\tilde{z}^T Q\tilde{z} + 2\beta\Big(\tilde{z}^T\Upsilon_o\tilde{z}\Big)^{\beta-1}\|\tilde{z}^T\Upsilon_o\|\|\Phi(\hat{z}) - \Phi(z)\| - 2\beta\Big(\tilde{z}^T\Upsilon_o\tilde{z}\Big)^{\beta-1}\tilde{z}^T\Upsilon_o L_{o_1}(L\tilde{z})^{\sigma} \\ & - 2\beta\Big(\tilde{z}^T\Upsilon_o\tilde{z}\Big)^{\beta-1}\tilde{z}^T\Upsilon_o L_{o_2}\tanh\left(L\tilde{z}/\rho\right) - 2\beta\Big(\tilde{z}^T\Upsilon_o\tilde{z}\Big)^{\beta-1}\|\tilde{z}^T\Upsilon_o\|\|\bar{\theta}\|.\end{aligned} \tag{29}$$

Invoking Assumptions 1 and 2 in (29) gives

$$\begin{aligned}\dot{V}_o(\tilde{z}(t)) \leq & -\beta\Big(\tilde{z}^T\Upsilon_o\tilde{z}\Big)^{\beta-1}\tilde{z}^T Q\tilde{z} + 2\beta\gamma\Big(\tilde{z}^T\Upsilon_o\tilde{z}\Big)^{\beta-1}\|\tilde{z}^T\Upsilon_o\|\|\tilde{z}\| - 2\beta\Big(\tilde{z}^T\Upsilon_o\tilde{z}\Big)^{\beta-1}\tilde{z}^T\Upsilon_o L_{o_1}L^{\sigma}\tilde{z}^{\sigma} \\ & + 2\beta\Big(\tilde{z}^T\Upsilon_o\tilde{z}\Big)^{\beta-1}\|\tilde{z}^T\Upsilon_o\|(-\|L_{o_2}\| + \|l_\theta\|)\,.\end{aligned} \tag{30}$$

If the norm of observer gain is chosen such as $\|L_{o_2}\| \geq l_\theta$, then it yields

$$\begin{aligned}\dot{V}_o(\tilde{z}(t)) &\leq -\beta\Big(\tilde{z}^T\Upsilon_o\tilde{z}\Big)^{\beta-1}\tilde{z}^T Q\tilde{z} + 2\beta\gamma\Big(\tilde{z}^T\Upsilon_o\tilde{z}\Big)^{\beta-1}\|\tilde{z}^T\Upsilon_o\|\|\tilde{z}\| - 2\beta\Big(\tilde{z}^T\Upsilon_o\tilde{z}\Big)^{\beta-1}\tilde{z}^T\Upsilon_o L_{o_1}L^{\sigma}\tilde{z}^{\sigma} \\ &\leq -\beta(\lambda_{min}(Q\Upsilon_o^{-1}) - 2\gamma)V_o(\tilde{z}(t)) - 2\beta\lambda_{min}(L_{o_1}L^{\sigma})V_o{}^{\frac{\beta+\sigma-1}{\beta}}(\tilde{z}(t)).\end{aligned} \tag{31}$$

Since $0 < \dfrac{\beta+\sigma-1}{\beta} < 1$, if the condition $\lambda_{min}(Q\Upsilon_o^{-1}) > 2\gamma$ holds, from Lemma1 the finite-time stability of the extended observer error system (24) is concluded. Therefore, the exact value of $z(t)$ is precisely estimated within t_r. Accordingly, applying the transformation matrix (21) to the (24), the estimated values of state vector x and lumped disturbance function $d(x,t)$ are extracted. □

Remark 5. *One of the characteristics of changing coordinates is that the estimation problem of the unknown states and unknown disturbance term is done by an extended state observer. The finite-time stability is obtained for the observer system as well.*

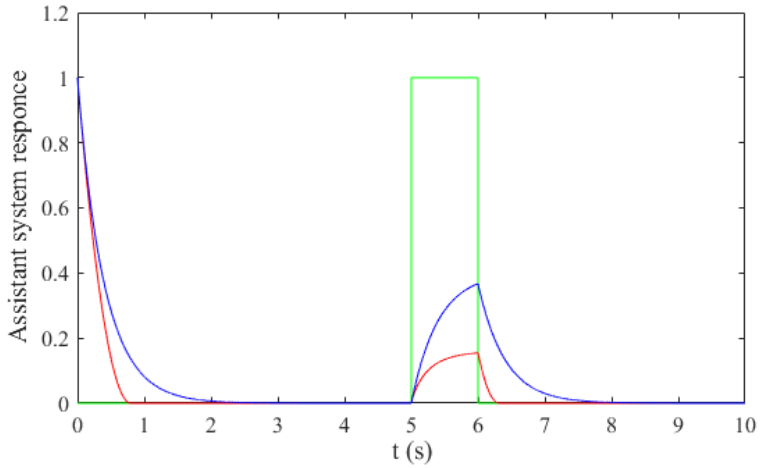

Figure 2: Performance evaluation of the assistant system (37) in 1-dimention as $\dot{h} = -k_h h^{\mu} + \delta_h$ with $k_h = 2.5$, $\mu = 0.5$ (red color), and $\mu = 1.0$ (blue color), in which δ_h is a disturbance function (green color), and its value is equal to 1 during time interval [5 6] s.

3.2. Finite-time robust fractional-order sliding mode-based tracking controller design

In this section, using the estimation results in the previous section, the estimated velocity states, $\hat{x}$, and the disturbance function, $\hat{d}(x,t)$, and based on the fractional calculus and a sliding-mode technique, a robust centralized controller is designed.

To take away input-delay from the calculations, and to facilitate the controller design, we apply Laplace transform to the delayed saturation function and then we use a Padé approximation technique as

$$\mathcal{L}\left[\text{sat}\left(\tau(t-t_d)\right)\right] = e^{-t_d\varsigma}\mathcal{L}\left[\text{sat}\left(\tau(t)\right)\right] \approx \frac{1-\frac{t_d\varsigma}{2}}{1+\frac{t_d\varsigma}{2}}\mathcal{L}\left[\text{sat}\left(\tau(t)\right)\right], \tag{32}$$

where $\varsigma \in \mathbb{C}$ is the Laplace complex variable and $\mathcal{L}[\cdot]$ is the Laplace transform operator. Equation (32) can be rewritten in terms of Laplace transform of a new state $v(t) \in R^{2m}$ as

$$\frac{1-\frac{t_d\varsigma}{2}}{1+\frac{t_d\varsigma}{2}}\mathcal{L}\left[\text{sat}\left(\tau(t)\right)\right] = \mathcal{L}\left[v(t)\right] - \mathcal{L}\left[\text{sat}\left(\tau(t)\right)\right], \tag{33}$$

where

$$\mathcal{L}\left[v(t)\right] = \frac{4}{2+t_d\varsigma}\mathcal{L}\left[\text{sat}\left(\tau(t)\right)\right]. \tag{34}$$

The equivalent of (34) in the time domain is

$$\dot{v}(t) = -\xi v(t) + 2\xi\,\text{sat}\left(\tau(t)\right), \tag{35}$$

where $\xi = 2/t_d$. On the other hand, from (32) and (33), one can write

$$\text{sat}\left(\tau(t-t_d)\right) = v(t) - \left[\tau(t) + \Delta\tau(t)\right], \tag{36}$$

where $\Delta\tau(t) = \text{sat}\left(\tau(t)\right) - \tau(t)$.

Now, let us introduce the following auxiliary system to deal with actuators saturation

$$\dot{h} = -K_h h^{\mu} + G\Delta\tau(t), \tag{37}$$

where $h \in R^{2n}$ is the state vector, $K_h \in R^{2n\times 2n}$ is a positive definite matrix, and $0 < \mu < 1$. System (37) has finite-time convergence property. The behaviour of one of its states during the specified time is illustrated in Fig. 2. Also, the performance of the auxiliary system (37), with $\mu = 0.5$, is compared with the same type of function with exponential convergence, $\mu = 1$, in terms of convergence rate and disturbance rejection properties. In this test, we assume that a disturbance with amplitude 1 affects the dynamics of the assistant system (37) within the time range $\begin{bmatrix}5 & 6\end{bmatrix}$ s, as also evident from Fig. 2. It is observed that the proposed system performs better than the exponential type in terms of disturbance rejection and convergence rate.

Applying the inverse coordinate transformation (21) to the observer system (23), and considering the two auxiliary systems (35) and (37), and also (36), the following set of systems is obtained which are employed within the controller design procedure

$$\begin{cases} \dot{\hat{x}} = \Omega\nabla H(\hat{x}) + Gv(t) - G\left[\tau(t) + \Delta\tau(t)\right] + \hat{d}(x,t) - TL_{o_1}\tilde{y}^{\sigma} - TL_{o_2}\tanh\left(\tilde{y}/\rho\right), \\ \dot{v}(t) = -\xi v(t) + 2\xi\left[\tau(t) + \Delta\tau(t)\right], \\ \dot{h} = -K_h h^{\mu} + G\Delta\tau(t), \end{cases} \tag{38}$$

where $T = \begin{bmatrix} I_{2n} & O_{2n\times 2n}\end{bmatrix}$.

Define the state tracking error as

$$e = \hat{x} - x_d - h + \frac{Gv(t)}{\xi}, \tag{39}$$

where $x_d \in R^{2n}$ is the desired trajectory vector. The proposed fractional-order sliding surface is then given by

$$s(t) = D^{\alpha-1}e + D^{\alpha-2}(K_{s_1}e + K_{s_2}e^{\zeta}), \tag{40}$$

where $K_{s_1} \in R^{2n\times 2n}$ and $K_{s_2} \in R^{2n\times 2n}$ are positive definite sliding surface gains, and $0 < \zeta < 1$. The convergence behavior of the tracking error for different values of α, $K_{s_1} = K_{s_2} = 1.5$, $\zeta = 0.75$, and for the case that the system is in the sliding mode, $s(t) = 0$, is exhibited in Fig. 3. It is obvious that, for $\alpha = 0.5$, an excellent convergence behaviour is observed and for $\alpha > 2$ the behaviour of tracking error goes to the unstable mode.

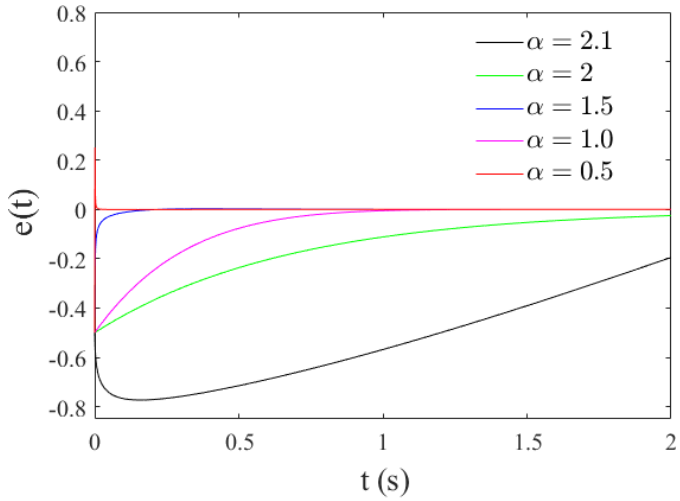

Figure 3: The convergence behavior of tracking errors for for different values of α, $K_{s_1} = K_{s_2} = 1.5$, and $\zeta = 0.75$.

When the controller puts the system into sliding mode (i.e., $s(t) = 0$), from the sliding dynamics $\dot{s}(t) = 0$, the following result can be extracted

$$D^{\alpha}e = -D^{\alpha-1}(K_{s_1}e + K_{s_2}e^{\zeta}). \tag{41}$$

Theorem 3. *Consider the sliding surface* (40)*. The sliding dynamics* (41) *is stable and its error states converge to equilibrium* $e(t) = 0$ *in finite time.*

Proof. Choose the following Lyapunov function candidate

$$V_s(e(t)) = \left(e^T\Upsilon_s e\right)^{\beta}, \tag{42}$$

where $\Upsilon_s \in R^{2n\times 2n}$. Taking its time derivative and using (41) yields

$$\begin{aligned}
\dot{V}_s(e) &= 2\beta\left(e^T\Upsilon_s e\right)^{\beta-1}e^T\Upsilon_s\dot{e}\\
&= 2\beta\left(e^T\Upsilon_s e\right)^{\beta-1}e^T\Upsilon_s D^{1-\alpha}D^{\alpha}e\\
&= -2\beta\left(e^T\Upsilon_s e\right)^{\beta-1}e^T\Upsilon_s K_{s_1}e - 2\beta\left(e^T\Upsilon_s e\right)^{\beta-1}e^T\Upsilon_s K_{s_2}e^{\zeta}\\
&\leq -2\beta\lambda_{min}(K_{s_1})\left(e^T\Upsilon_s e\right)^{\beta} - 2\beta\lambda_{min}(K_{s_2})\left(e^T\Upsilon_s e\right)^{\beta-1}e^T\Upsilon_s e^{\zeta}\\
&= -2\beta\left[\lambda_{min}(K_{s_1})V_s(e) + \lambda_{min}(K_{s_2})V_s^{\frac{\beta+\zeta-1}{\beta}}(e)\right].
\end{aligned} \tag{43}$$

Since $0 < \left(\frac{\beta+\zeta-1}{\beta}\right) < 1$, the finite-time stability is concluded from Lemma1 and the reaching time can be calculated using (12) and (13). □

Notice that the time derivative of $s(t)$ in (40) is

$$\dot{s}(t) = D^1 s(t) = D^{\alpha-1}\left[\dot{e} + (K_{s_1} e + K_{s_2} e^{\zeta})\right]. \tag{44}$$

In the following theorem, the structure of the proposed controller and the stability results of the closed-loop system (38) are provided.

Theorem 4. *Consider a set of dynamical systems including the estimated dynamics of a mechanical system in the pH form and two auxiliary systems to cope with input delay and actuators saturation as given in* (38)*. The following fractional-order sliding mode controller*

$$\begin{aligned}\tau(t) = -G^{\dagger}\Big(&\Omega\nabla H(\hat{x}) + \hat{d}(x,t) - TL_{o_1}\tilde{y}^{\sigma} - TL_{o_2} tanh\,(\tilde{y}/\rho) - \dot{x}_d + K_h h^{\mu} + \frac{\dot{G}v(t)}{\xi} + (K_{s_1} e + K_{s_2} e^{\zeta}) \\ &+ D^{1-\alpha}\left[K_{s_3} s + K_{s_4} s^{\eta}\right]\Big),\end{aligned} \tag{45}$$

where the † symbol stands for the pseudo-inverse operation, $K_{s_3} \in R^{2n\times 2n}$ and $K_{s_4} \in R^{2n\times 2n}$ are two positive definite matrices, and $0 < \eta < 1$, guarantees the finite time stability of the closed-loop system.

Proof. Taking the time derivative of (39) and considering the sliding dynamic (44) give

$$\dot{s}(t) = D^{\alpha-1}\left[\dot{\hat{x}} - \dot{x}_d - \dot{h} + \frac{\dot{G}v(t)}{\xi} + \frac{G\dot{v}(t)}{\xi} + (K_{s_1} e + K_{s_2} e^{\zeta})\right]. \tag{46}$$

Substituting the dynamics of $\hat{x}$, h, and $v(t)$ from (38) into (46) yields

$$\begin{aligned}\dot{s}(t) = D^{\alpha-1}\Big[&\Omega\nabla H(\hat{x}) + Gv(t) - G\left[\tau(t) + \Delta\tau(t)\right] + \hat{d}(x,t) - TL_{o_1}\tilde{y}^{\sigma} - TL_{o_2}\tanh\left(\tilde{y}/\rho\right) - \dot{x}_d + K_h h^{\mu} \\ &- G\Delta\tau(t) + \frac{\dot{G}v(t)}{\xi} - Gv(t) + 2G\left[\tau(t) + \Delta\tau(t)\right] + (K_{s_1} e + K_{s_2} e^{\zeta})\Big].\end{aligned} \tag{47}$$

Replacing the controller (45) into (47) gives

$$\dot{s}(t) = -K_{s_3} s - K_{s_4} s^{\eta}. \tag{48}$$

Now, let us choose the Lyapunov function equal to the energy of closed-loop system as

$$V_c(s(t)) = H_c(s(t)) = \left(s^T \Upsilon_c s\right)^{\beta}, \tag{49}$$

where $\Upsilon_c \in R^{2n\times 2n}$. Finally, taking the time derivative of (49) along the sliding dynamics (48) gives

$$\begin{aligned}\dot{V}_c(t) &= 2\beta\left(s^T\Upsilon_c s\right)^{\beta-1} s^T\Upsilon_c\dot{s} \\ &= -2\beta\left(s^T\Upsilon_c s\right)^{\beta-1} s^T\Upsilon_c K_{s_3} s - 2\beta\left(s^T\Upsilon_c s\right)^{\beta-1} s^T\Upsilon_c K_{s_4} s^{\eta} \\ &\le -2\beta\lambda_{min}(K_{s_3})\left(s^T\Upsilon_c s\right)^{\beta} - 2\beta\lambda_{min}(K_{s_4})\left(s^T\Upsilon_c s\right)^{\beta-1} s^T\Upsilon_c s^{\eta} \\ &= -2\beta\left[\lambda_{min}(K_{s_3})V_c(s) + \lambda_{min}(K_{s_4})V_c^{\frac{\beta+\eta-1}{\beta}}(s)\right].\end{aligned} \tag{50}$$

Since $0 < \left(\frac{\beta+\eta-1}{\beta}\right) < 1$, the finite-time stability of the closed-loop system is achieved from Lemma1. □

Remark 6. *Using fractional calculus in sliding surface* (40) *and a central controller* (45) *provides better flexibility to shape the trajectory tracking response. Compared with the integer-order sliding mode-based robust control technique in [49], the fractional-order sliding mode control scheme proposed in this paper has some superiority in a fast position and velocity tracking performance and high control accuracy.*

3.3. Extension to the case of unknown input delay

In this section, the results obtained within Section 3.1 and Section 3.2 are extended to those pH systems with unknown time delay.

For unknown time delay, (36) can be rewritten as

$$\text{sat}\,(\tau_z(t-t_d)) = v_u(t) - \text{sat}(\tau_z(t)), \tag{51}$$

where $v_u \in R^{4m}$ is the output of the following linear system

$$\dot{v}_u(t) = -k_u v_u(t) + f_u, \tag{52}$$

where $k_u \in R$ is a positive scalar, and $f_u = (k_u - \xi_u)v_u + 2\xi\text{sat}\,(\tau_z(t)) \in R^{4m}$ is an unknown function. Considering (51) and (52), equation (22) can be transformed to

$$\begin{cases} \dot{z}_u = A_u z_u + \Phi_u(z_u) + \mathcal{G}_u \text{sat}\,(\tau_u(t)) + \bar{\theta}_u, \\ y_u = L_u z_u, \end{cases} \tag{53}$$

where $z_u = \begin{bmatrix} z^T & v_u^T \end{bmatrix}^T \in R^{4(n+m)}$, $\Phi_u(z_u) = \begin{bmatrix} \phi^T(z) & 0_{4m}^T \end{bmatrix}^T \in R^{4(n+m)}$, $\mathcal{G}_u = \text{diag}(\mathcal{G}, 0_{4m\times 2m}) \in R^{4(n+m)\times 4m}$, $L_u = \begin{bmatrix} L & O_{n\times 4m} \end{bmatrix} \in R^{n\times 4(n+m)}$, $\bar{\theta}_u = \begin{bmatrix} \bar{\theta}^T & f_u^T \end{bmatrix}^T \in R^{4(n+m)}$, $\tau_u = \begin{bmatrix} \tau_z^T & \tau_z^T \end{bmatrix}^T \in R^{4m}$, and $A_u = \begin{pmatrix} A & \mathcal{G} \\ 0_{4m\times 4n} & k_u I_{4m} \end{pmatrix} \in R^{4(n+m)\times 4(n+m)}$.

For the system (53), the proposed state and disturbance observer has the following structure

$$\begin{cases} \dot{\hat{z}}_u = A_u \hat{z}_u + \Phi_u(\hat{z}_u) + \mathcal{G}_u \text{sat}\,(\tau_u(t)) - L_{o_{1u}} \tilde{y}_u^{\sigma} - L_{o_{2u}} \tanh\,(\tilde{y}_u/\rho)\,, \\ \hat{y}_u = L_u \hat{z}_u, \end{cases} \tag{54}$$

where $\hat{z}_u \in \mathbb{R}^{4n+4m}$ is the estimated value of z_u, $\hat{y}_u \in \mathbb{R}^n$ is the estimated value of y_u, $\tilde{y}_u = \hat{y}_u - y_u \in \mathbb{R}^n$ is the output estimation error, and $L_{o_{1u}} \in R^{(4n+4m)\times n}$ and $L_{o_{2u}} \in R^{(4n+4m)\times n}$ are the observer gain matrices.

As described in Section 3.1, the inverse coordinate transformation can be applied to obtain the estimated values of the system state x_u, $\hat{x}_u$, assistant system state v_u, $\hat{v}_u$, and unknown function f_u, $\hat{f}_u$, as

$$\begin{cases} \dot{\hat{x}}_u = \Omega\nabla H(\hat{x}_u) + G\hat{v}_{u_1}(t) - G\,[\tau(t) + \Delta\tau(t)] + \hat{d}_u(x,t) - TL_{o_{1u}}\tilde{y}_u^{\sigma} - TL_{o_{2u}} \tanh\,(\tilde{y}_u/\rho)\,, \\ \dot{\hat{v}}_{u_1}(t) = -k_u \hat{v}_{u_1}(t) + \hat{f}_{u_1}, \end{cases} \tag{55}$$

where the subscript u stands for the unknown delay case, $\hat{v}_u = \begin{bmatrix} \hat{v}_{u_1}^T(t) & \hat{v}_{u_2}^T(t) \end{bmatrix}^T$ with $\hat{v}_{u_1}^T(t), \hat{v}_{u_2}^T(t) \in R^{2m}$, and $\hat{f}_u = \begin{bmatrix} \hat{f}_{u_1}^T(t) & \hat{f}_{u_2}^T(t) \end{bmatrix}^T$ with $\hat{f}_{u_1}^T(t), \hat{f}_{u_2}^T(t) \in R^{2m}$.

For the unknown input delay case, the state tracking error, e_u, and fractional-order sliding surface, $s_u(t)$, are defined as

$$e_u(t) = \hat{x}_u - x_d + h + \frac{G\hat{v}_{u_1}(t)}{k_u}, \tag{56}$$

$$s_u(t) = D^{\alpha-1}e_u + D^{\alpha-2}(K_{s_1}e_u + K_{s_2}e_u^{\zeta}), \tag{57}$$

where h is the state vector of the assistant system (37). The fractional-order sliding mode controller (45) is modified as

$$\begin{aligned} \tau(t) = -G^{\dagger}\Big(&\Omega\nabla H(\hat{x}_u) + \hat{d}_u(x,t) - TL_{o_{1u}}\tilde{y}_u^{\sigma} - TL_{o_{2u}}\tanh\,(\tilde{y}_u/\rho) - \dot{x}_d \\ &- K_h h^{\mu} + \frac{G\hat{f}_{u_1}(t)}{k_u} + \frac{G\dot{v}_{u_1}(t)}{k_u} + (K_{s_1}e_u + K_{s_2}e_u^{\zeta}) + D^{1-\alpha}\left[K_{s_3}s_u + K_{s_4}s_u^{\eta}\right]\Big), \end{aligned} \tag{58}$$

Note that the observer (54), the fractional-order sliding surface (57), and the closed-loop system under the controller (58) are finite-time stable, and the stability can be proven as explained in Theorems 2, 3, and 4.

3.4. Stability analysis including impacts

In subsections 3.1 and 3.2, the general form for the time derivatives of the Lyapunov functions (27), (42), and (49) were obtained as in (12). Assume that the k^{th} impact occurs at time $t = t_k$. Let $t \in [t_k, t_{k+1})$. Integrating (12) from t_k to t yieds

$$V^{1-c}(t) \leq V^{1-c}(t_k)e^{-a(1-c)(t-t_k)} - \frac{b}{a}[1 - e^{-a(1-c)(t-t_k)}]. \tag{59}$$

For stability analysis, taking into account the hybrid nature of the system due to impacts, the relation between the Lyapunov function before, $V_{t_k}^-$, and after, $V_{t_k}^+$, the impact times should be extracted. Having in mind Remark 3 and considering (31), (43), and (50), the matrices Υ_o, Υ_s, and Υ_c are selected as

$$\begin{cases} \Upsilon_{o_k}(l_1, l_1) \leq \varrho_o^{\frac{1}{\beta}} \Upsilon_{o_{k-1}}(l_1, l_1), \\ \Upsilon_{s_k}(l_2, l_2) \leq \varrho_s^{\frac{1}{\beta}} \Upsilon_{s_{k-1}}(l_2, l_2), \\ \Upsilon_{c_k}(l_2, l_2) \leq \varrho_c^{\frac{1}{\beta}} \Upsilon_{c_{k-1}}(l_2, l_2), \end{cases} \tag{60}$$

where Υ_{o_k}, Υ_{s_k}, and Υ_{c_k} are the values of Υ_o, Υ_s, and Υ_c at $t = t_k$, while $\varrho_o, \varrho_s, \varrho_c > 1$, $l_1 = 1, \ldots, 4n$, and $l_2 = 1, \ldots, 2n$. Conditions (60) ensure the decreasing property for three matrices Υ_o, Υ_s, and Υ_c. Through these choices, the following result for V_o, V_s and V_c can be obtained

$$\begin{cases} V_o(t_k^+) \leq \varrho_o V_o(t_k^-), \\ V_s(t_k^+) \leq \varrho_s V_s(t_k^-), \\ V_c(t_k^+) \leq \varrho_c V_c(t_k^-). \end{cases} \tag{61}$$

Therefore, one can write

$$V(t_k^+) \leq \varrho V(t_k^-). \tag{62}$$

Combining (59) and (62) yields

$$\begin{aligned} V^{1-c}(t) &\leq \varrho V^{1-c}(t_k^-)e^{-a(1-c)(t-t_k)} - \frac{b}{a}[1 - e^{-a(1-c)(t-t_k)}] \\ &\leq \varrho V^{1-c}(t_{k-1})e^{-a(1-c)(t-t_{k-1})} - \frac{b}{a}[1 - e^{-a(1-c)(t-t_{k-1})}] - \frac{b}{a}\varrho[1 - e^{-a(1-c)(t-t_{k-1})}] \\ &\leq ... \\ &\leq \varrho^{n_\sigma} V^{1-c}(t_0)e^{-a(1-c)(t-t_0)} - \frac{b}{a}[1 - e^{-a(1-c)(t-t_k)}] - \ldots - \frac{b}{a}\varrho^{n_\sigma}[1 - e^{-a(1-c)(t-t_0)}] \\ &\leq \varrho^{n_\sigma} V^{1-c}(t_0)e^{-a(1-c)n_\sigma t_N} - \frac{b}{a}\frac{\varrho e^{-a(1-c)t_N}(e^{-a(1-c)t_N} - 1)}{\varrho e^{-a(1-c)t_N}}[1 - \varrho^{n_\sigma} e^{-a(1-c)n_\sigma t_N}], \end{aligned} \tag{63}$$

where $t_N = t_k - t_{k-1}$ and $n_\sigma > 0$ is the number of switching times. The bound in (63) can be rewritten as

$$V^{1-c}(t) \leq \Psi \varrho^{n_\sigma} e^{-a(1-c)n_\sigma T_N} - \Phi, \tag{64}$$

where $\Phi = \frac{b}{a}\frac{e^{-a(1-c)t_N} - 1}{\varrho e^{-a(1-c)t_N} - 1}$ and $\Psi = V^{1-c}(t_0) - \varrho\Phi$. If $\varrho e^{-a(1-c)t_N} - 1 < 0$, then the upper-bound of $V(t)$ will be positive

$$V(t) \leq \left[\Psi \varrho^{n_\sigma} e^{a(1-c)n_\sigma T_N} - \Phi\right]^{\frac{1}{1-c}} = b_2. \tag{65}$$

This means that the stability of the closed-loop system as well as the extended observer dynamics (24) is preserved not only during free motion phase, but also in presence of the impact. Therefore, using Definition 1, these two systems are finite-time stable.

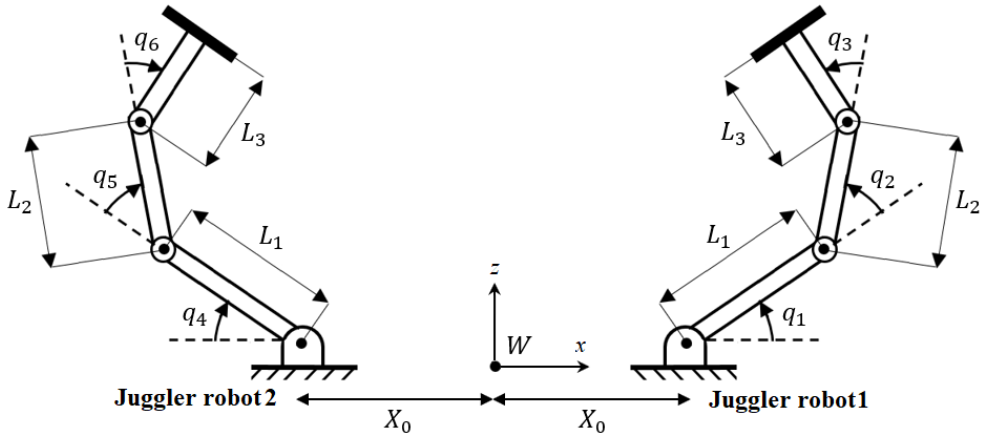

Figure 4: The geometrical structure of two juggler robots with three degrees of freedom.

4. Numerical simulations

In this section, the general theoretical results obtained in the previous sections are validated on an appealing hybrid system: the ball-playing juggler robot. Peculiarities of such a system were provided in Section 1.1.

4.1. Kinematic and dynamic of a ball-juggler robot

The geometrical structure of each juggler robot is shown in Fig. 4. The end-effector position of the first juggler robot can be retrieved through the following geometric relationships

$$\begin{cases} x_e = L_1 \cos(q_1) + L_2 \cos(q_1 + q_2) + L_3 \cos(q_1 + q_2 + q_3) + X_0, \\ z_e = L_1 \sin(q_1) + L_2 \sin(q_1 + q_2) + L_3 \sin(q_1 + q_2 + q_3), \end{cases} \tag{66}$$

where $q_1, q_2, q_3 \in \mathbb{R}$ are the joint angles of the juggler robot 1. Similar expressions can be obtained for the second juggler robot with the related joint angles $q_4, q_5, q_6 \in \mathbb{R}$. Using inverse-kinematic calculations [50], the values of the joint angles for the first juggler robot can be obtained as

$$\begin{cases} \varphi = \text{atan2}(\dfrac{x_e - X_0}{z_e}), \\ x_p = x_e - X_0 - L_3 \cos(\varphi), \\ z_p = z_e - L_3 \sin(\varphi), \\ c_2 = \dfrac{x_p^2 + z_p^2 - {L_1}^2 - {L_2}^2}{2L_1 L_2}, \\ s_2 = \pm\sqrt{1 - {c_2}^2}, \\ q_2 = \text{atan2}(s_2, c_2), \\ q_1 = \text{atan2}(z_p, x_p) - \text{atan2}(L_2 s_2, L_1 + L_2 c_2), \\ q_3 = \varphi - q_1 - q_2. \end{cases} \tag{67}$$

where the two solutions identified by the + and − signs correspond to the "elbow up" and "elbow down" configurations, respectively. The closest configuration to the actual one is selected. Similar expressions can be obtained for the second juggler robot.

The dynamic equation of the juggler robots can be extracted using Euler-Lagrange method [50]. The details of the mass and inertia matrix, the Coriolis matrix, and the vector of gravitational terms for the first juggler robot are given in the Appendix A.

4.2. Dynamic equations of ball motion

Three forces affect the dynamic behavior of the ball during the free-flight motion. They are namely the air resistance force, $F_a \in \mathbb{R}^3$, the Magnus force, $F_m \in \mathbb{R}^3$, and the gravitational force $F_g \in \mathbb{R}^3$. It can be expressed by [27]

$$m\dot{v}_b = F_a + F_m + F_g \tag{68}$$

where

$$F_a = -\frac{1}{2}\rho s_a c_a \|v_b\| v_b, \tag{69}$$

$$F_m = \rho \omega_b r_b s_a c_l v_b, \tag{70}$$

$$F_g = [0, 0, -m_b g]^T, \tag{71}$$

where $\rho > 0$ is the air density, $c_a > 0$ is the drag coefficient, $v_b = \begin{bmatrix} v_{b_x} & v_{b_y} & v_{b_z} \end{bmatrix}^T \in R^3$ is the translational velocity of the ball, $\|\cdot\| > 0$ is the Eucledian norm operator, $\omega_b \in \mathbb{R}^3$ is the rotational velocity of the ball, $c_l > 0$ is the lift coefficient, and g is the gravity acceleration. Finally, $s_a > 0$, $m_b > 0$, and $r_b > 0$ are the effective contact area, the mass, and the radius, respectively. According to [27], the motion of the ball can be represented by the following equations

$$\begin{bmatrix} \dot{x}_b \\ \dot{y}_b \\ \dot{z}_b \\ \dot{v}_{b_x} \\ \dot{v}_{b_y} \\ \dot{v}_{b_z} \end{bmatrix} = \begin{bmatrix} v_{b_x} \\ v_{b_y} \\ v_{b_z} \\ -\frac{1}{2m}\rho s_a (c_a \|v_b\| - 2\omega_b r_b c_l) v_{b_x} \\ -\frac{1}{2m}\rho s_a (c_a \|v_b\| - 2\omega_b r_b c_l) v_{b_y} \\ -\frac{1}{2m}\rho s_a (c_a \|v_b\| - 2\omega_b r_b c_l) v_{b_z} - g \end{bmatrix}. \tag{72}$$

where x_b, y_b, and z_b are the position of the ball in x, y, and z directions, respectively.

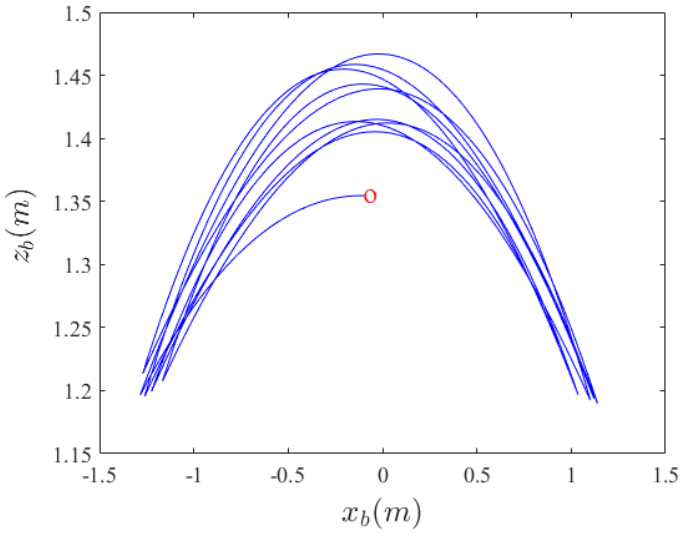

Figure 5: Measured ball motion trajectory during ball-playing game by two juggler robots. Red marker O indicates the initial position of the ball.

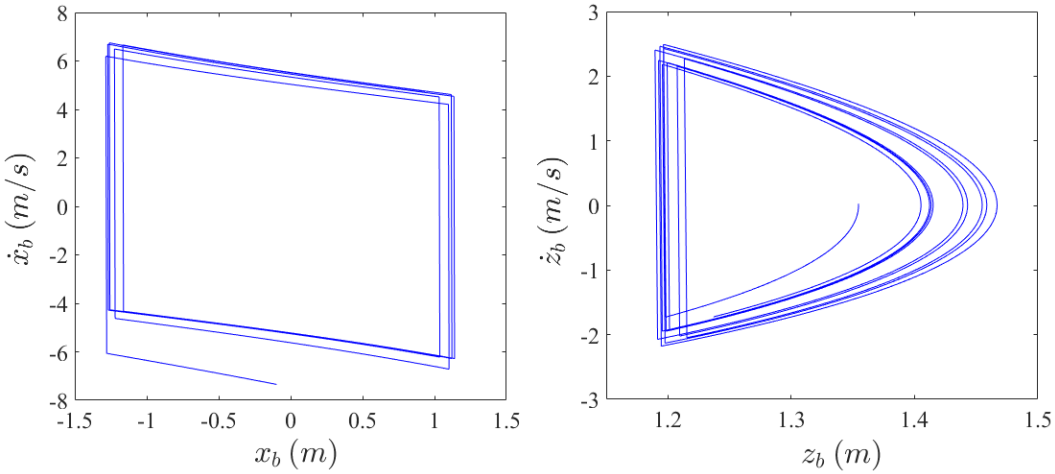

Figure 6: Phase portraits of the ball states.

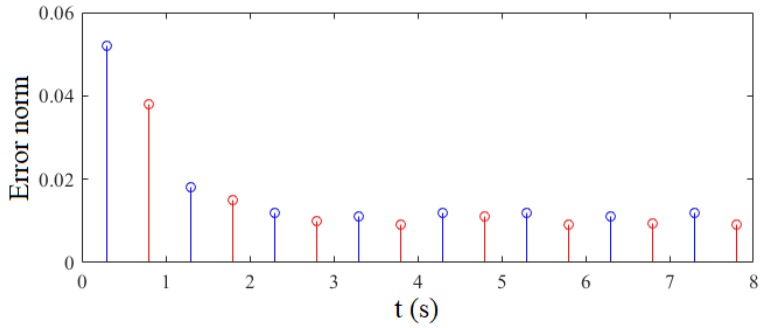

Figure 7: Norm of the error between desired, p_{b_d}, and measured, p_{b_m}, ball trajectories at impact times. Blue and red circles indicate the the errors caused by the first and second juggler robots, respectively.

After an impact, the translational and rotational velocities of the ball are updated according to the following equation [25]

$$v_b^+ = v_r + R_{rot}A_{vv}R_{rot}^T(v_b^- - v_r) + R_{rot}A_{vw}R_{rot}^T\omega_b^- \tag{73}$$

$$\omega_b^+ = R_{rot}A_{wv}R_{rot}^T(v_b^- - v_r) + R_{rot}A_{ww}R_{rot}^T\omega_b^- \tag{74}$$

where $v_r \in R^3$ is the velocity of the racket attached to the juggler robot's end-effector at the hitting time, $R_{rot} \in \mathrm{SO}(3)$ is the rotation matrix of the racket frame with respected to the world frame, $A_{vv} = \mathrm{diag}(1-k_v, 1-k_v, -e_r)$, $A_{vw} = k_v r S_{rb}$, $A_{wv} = -k_w r S_{rb}$, $A_{ww} = \mathrm{diag}(1-k_w r^2, 1-k_w r^2, 1)$, and

$$S_{rb} = \begin{bmatrix} 0 & 1 & 0 \\ -1 & 0 & 0 \\ 0 & 0 & 0 \end{bmatrix}.$$

According to [27], the values of the parameters were chosen as $m_b = 2.7\times10^{-3}$, $e_r = 7.3\times10^{-1}$, $k_v = 6.15\times10^{-1}$, $k_w = 2.57\times10^{3}$, and $r = 2\times10^{-2}m$ in the carried out simulations.

4.3. Dynamic equations of ball-juggler robotic system in pH form

Considering the structure of the juggler robots in Fig. 4, the ball dynamics in (72) and its velocity resetting condition in (73) and (74), the state vectors x_1 and x_2, ∇H, G, Δ_p, and Ω in (10) take the following values:

$$x_1 = \begin{bmatrix} p_b^T & q_{j_1}^T & q_{j_2}^T \end{bmatrix}^T,$$

$$x_2 = \begin{bmatrix} m_b v_b^T & (M_1(q_{j_1})\dot{q}_{j_1})^T & (M_2(q_{j_2})\dot{q}_{j_2})^T \end{bmatrix}^T,$$

$$\nabla H = \begin{bmatrix} (\nabla_{x_b} H_b)^T & (\nabla_{q_{jr}} H_{jr})^T & (\nabla_{v_b} H_b)^T & (\nabla_{p_{jr}} H_{jr})^T \end{bmatrix}^T,$$

$$G = \begin{bmatrix} O_{6\times 12} & I_6 \end{bmatrix}^T,$$

$$\Delta_p = \begin{bmatrix} (p_b^-)^T & (q_{jr}^-)^T & (m_b v_b^+)^T & p_{jr}^+ \end{bmatrix}^T,$$

$$\Omega = \begin{bmatrix} O_{9\times 9} & I_9 \\ -I_9 & O_{9\times 9} \end{bmatrix},$$

where $p_b = \begin{bmatrix} x_b & y_b & z_b \end{bmatrix}^T \in R^3$ is the ball position vector, $q_{j_1} = \begin{bmatrix} q_1 & q_2 & q_3 \end{bmatrix}^T \in \mathbb{R}^3$ and $q_{j_2} = \begin{bmatrix} q_4 & q_5 & q_6 \end{bmatrix}^T \in \mathbb{R}^3$, $M_1(q_{j_1}) \in R^{3\times 3}$ and $M_2(q_{j_2}) \in R^{3\times 3}$ are the mass and inertia matrix of the first and the second juggler robots, respectively, and $H_b = \frac{1}{2} m_b v_b^T v_b + V_b(x_b)$ is the Hamiltonian function of the ball, in which $V_b(x_b)$ is its potential energy. Finally, $H_{jr} \in \mathbb{R}$ is the Hamiltonian function of the whole juggler robot system and it is defined as in (4), $q_{jr} = \begin{bmatrix} q_{j_1}^T & q_{j_2}^T \end{bmatrix}^T \in \mathbb{R}^6$, and $p_{jr} = \begin{bmatrix} p_{j_1}^T & p_{j_2}^T \end{bmatrix}^T \in \mathbb{R}^6$ is the momentum vector of the two juggler robots. The values of p_{jr}^+ in the impact times $t = t_k$ are calculated as explained after (10).

For the first ball-juggler robot, the impact condition is defined with respect to the state vector x_1 as

$$\begin{cases} \vartheta_1(x_1) = x_b - \Big[L_1 \cos(q_1) + L_2 \cos(q_1 + q_2) + L_3 \cos(q_1 + q_2 + q_3) + X_0 \Big] = 0, \\ \vartheta_2(x_1) = z_b - \Big[L_1 \sin(q_1) + L_2 \sin(q_1 + q_2) + L_3 \sin(q_1 + q_2 + q_3) \Big] = 0, \end{cases} \tag{75}$$

Note that the similar expressions can be obtained for the second juggler robot.

4.4. Analysis of the obtained results

The lengths of the links of the first juggler robot are chosen as $L_1 = 1$ m, $L_2 = 0.75$ m, and $L_3 = 0.25$ m. The mass of all three links is 1 kg, i.e. $m_1 = m_2 = m_3 = 1$ kg. The gravitational acceleration, g, is 9.81 m/s^2.

The designed parameters for the fractional-order sliding mode controller are experimentally tuned as $\alpha = 1.75$, $\zeta = 0.75$, $\eta = 5$, $\mu = 0.5$, $K_{s_1} = 15I_{18}$, $K_{s_2} = 5I_{18}$, $K_{s_3} = 15I_{18}$, $K_{s_4} = 10I_{18}$, and $K_h = 2.5I_{18}$. For the extended state observer, the assigned coefficients are $K_x = 5I_{18}$, $\Lambda = 2I_{18}$, $\Upsilon_o = (2.5e^{-0.25t} + 2.5)I_{36}$, $\Upsilon_s = (2.5e^{-0.25t} + 2.5)I_{18}$, $L_{o_1} = 25\begin{bmatrix} I_9 & I_9 & I_9 & I_9 \end{bmatrix}^T$, $L_{o_2} = 15\begin{bmatrix} I_9 & I_9 & I_9 & I_9 \end{bmatrix}^T$, $\rho = 0.01$, and $\sigma = 0.85$.

The upper and lower saturation levels for each juggler robot are chosen as $\tau_{max} = \begin{bmatrix} 15 & 25 & 25 \end{bmatrix}^T$ Nm and $\tau_{min} = -\tau_{max}$, respectively. Input delay was set to $t_d = 10^{-2}$ s. The renaming and resetting matrix of the juggler robots are $\Delta_{n_1} = I_3$, $\Delta_{n_2} = I_3$, $\Delta_{s_1} = I_3$, and $\Delta_{s_2} = I_3$. The lumped unknown function $d(x, t)$ is composed of two terms: the first term is related to the parameter uncertainties, $d(x) \in \mathbb{R}^{2n}$, and the second term is the external disturbance, $d(t) \in \mathbb{R}^{2n}$, i.e., $d(x, t) = d(x) + d(t)$. It is assumed that the uncertainty function of the juggler robotic system is provided from a ten percent deviation of the nominal value of the Hamiltonian's gradient $\nabla H(x)$ (i.e., $d(x) = \pm 0.1 \nabla H(x)$). The external disturbance vector affecting the dynamic of each juggler robot is selected as $d(t) = \begin{bmatrix} 7.5\sin(1.5t) & 0 & 5\cos(2t) \end{bmatrix}^T$.

The juggler robot dynamics, the proposed fractional-order controller, and the extended-state observer were implemented in the MATLAB/Simulink environment and solved through the Runge–Kutta algorithm with sampling time 10^{-3} s. The Caputo fractional derivative is employed in this simulation. The trajectories of the ball are generated using (72) , (73), and (74). The juggler robot uses the information of the ball trajectory to regulate the positions and the orientations of the end-effectors [51]. Based on the end-effector positions and orientations, and using inverse-kinematic calculations (67), the desired trajectories of the joints are produced.

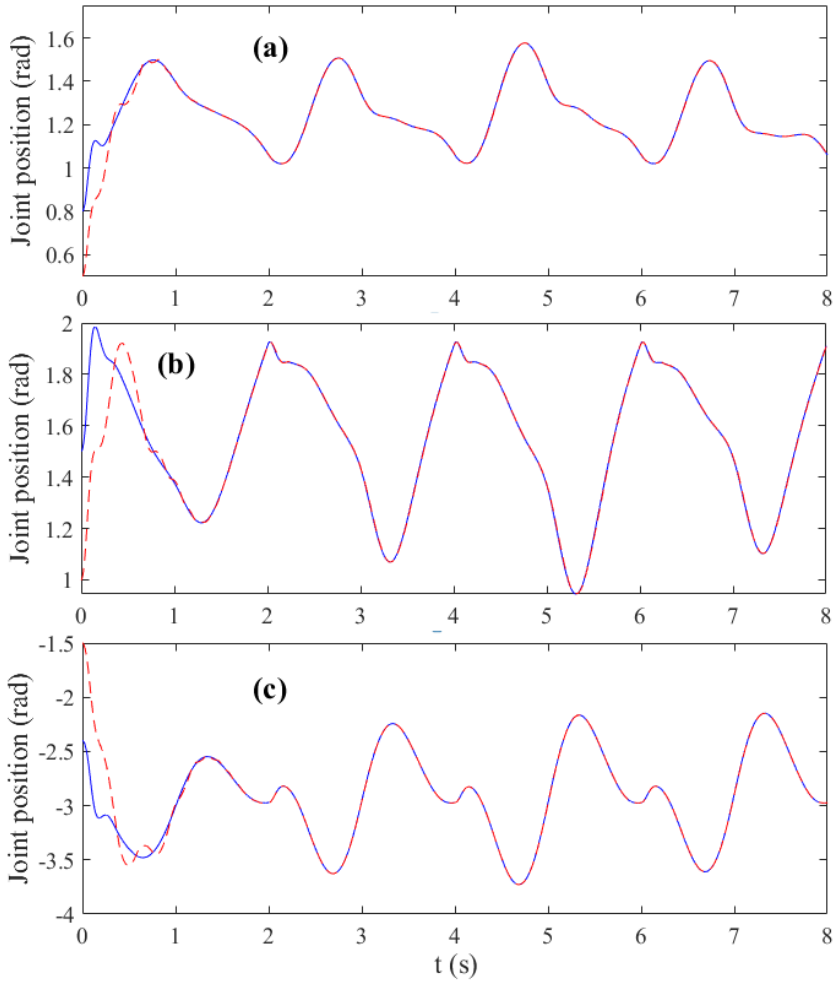

Figure 8: Desired, blue line, and measured, red dashed line, angular joint positions of the first juggler robot: (a) q_{d_1} and q_{m_1}, (b) q_{d_2} and q_{m_2}, and (c) q_{d_3} and q_{m_3}.

Here, the controller objective forces the states of the juggler robots to the desired trajectories to hit the ball in appropriate positions, which results in controlling the ball's motion. The measured ball motion trajectory (the so-called juggling pattern) is plotted in Fig. 5 in the $x-z$ plane. The phase portraits of the ball states are plotted in Fig. 6. The norm of the error between the desired, p_{b_d}, and the measured, p_{b_m}, ball trajectories at the impact times for the first (blue circles) and the second (red circles) juggler robots is depicted in Fig. 7. It is observed that the error is a little high at the first impact time only. As for the other impact times, the error stays around 0.01 and 0.012 m. Therefore, the juggling pattern results in the desired repetitive action for the whole playing time.

The results of the proposed framework are displayed from Fig. 8 to Fig. 14. In detail, the time responses of the measured and desired robot joint position trajectories are plotted in Fig. 8. The results are representative of the good convergence of the measured joint position states to their desired trajectories. The time response of the extended state observer is plotted in Fig. 9, showing that the proposed observer estimates the system states with good precision. Figure 10 shows the behavior of the estimated position tracking errors using the extended-state observer. As we expected, the position tracking errors rapidly tend to zero, indicating that the state reconstruction objective is achieved well. The sliding variables $s_i(t), i = 1, 2, 3$ are shown in Fig. 11. Note that, to eliminate the adverse effects of the time delays in control signals and saturation constraints, the auxiliary variables v and h were included in the definition of the tracking error e in (39). For this reason, the sliding variables converge to a region near the origin. To further

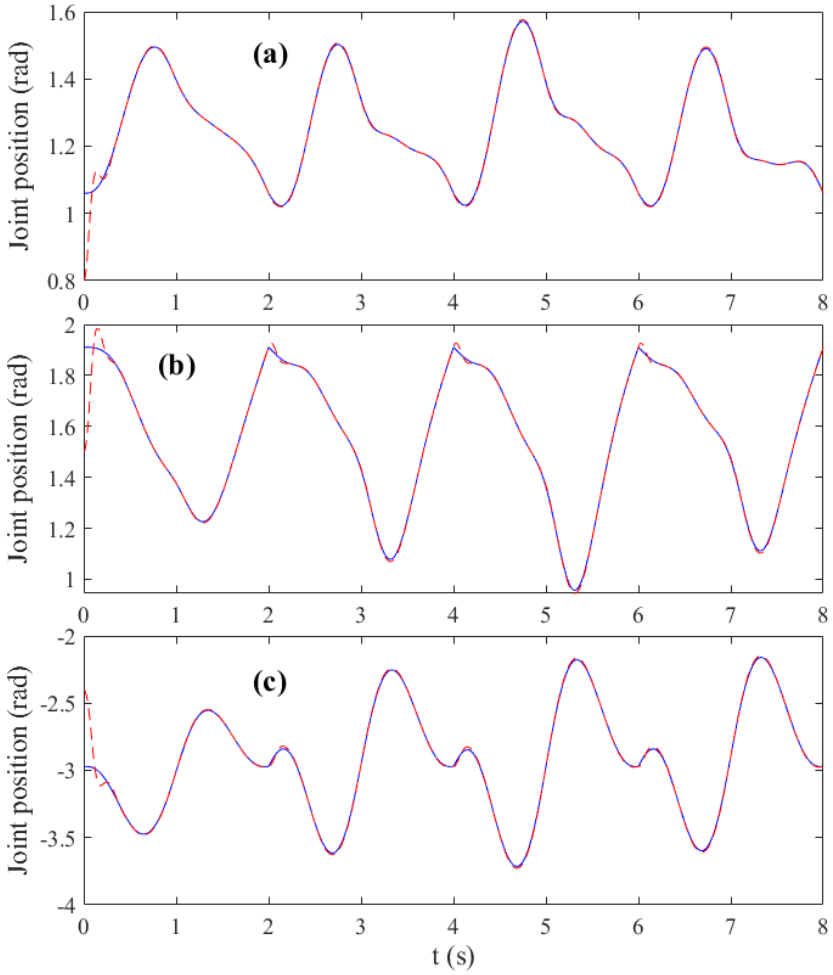

Figure 9: Measured, blue line, and estimated, red dashed line, angular joint positions of the first juggler robot: (a) q_{m_1} and $\hat{q}_{m_1}$, (b) q_{m_2} and $\hat{q}_{m_2}$, and (c) q_{m_3} and $\hat{q}_{m_3}$.

illustrate the finite-time stability, the behaviour of the energy function $V_s(t)$ is plotted in Fig. 12. It can be seen that the energy of $s(t)$ becomes zero before a finite-time. Fig. 13 illustrates the phase portraits between the states q_i and $\dot{q}_i$, $i = 1, 2, 3$. They show that the system responses follow the desired phase portraits. After a short time, the states of the juggler robot follow the desired stable limit-cycles: it can be thus concluded that the repetitive juggling actions are successfully performed. Control efforts τ_1 to τ_3 are plotted in Fig. 14(a)-(c). It is observed that, after a short time, the control signals are confined inside predefined saturation limits, and without any chattering effects, the signals demonstrate continuous behaviors.

To investigate carefully and for comparison study, the advantages of two other controllers, namely, integral sliding mode control (ISMC) [49] and fractional-order sliding mode control (FOSMC) [52], were employed in the control of a robotic juggler system. These controllers were proposed to stabilize the general class of uncertain Hamiltonian systems and balance a two-wheeled autonomous vehicle, respectively. It is assumed that the non-zero mean disturbances appear in the dynamic of $\dot{q}_2$ within the time interval $t \in [2, 6]$ s as $d_2(t) = 7.5 + 10\sin(5t)$, and in the dynamic of $\dot{q}_3$ within the time interval $t \in [1, 5]$ s as $d_3(t) = 10$. The results of this comparative study are shown from Fig.Fig. 15 to Fig. 17. The time responses of the angular position tracking errors and the angular velocity tracking errors are shown in Fig. 15 and Fig. 16, respectively. Our proposed control technique has good disturbance rejection capability and provides a superior control performance with a faster convergence rate and higher tracking accuracy. Note that, although the tracking performances of ISMC and FOSMC might be improved by increasing their control gains, this

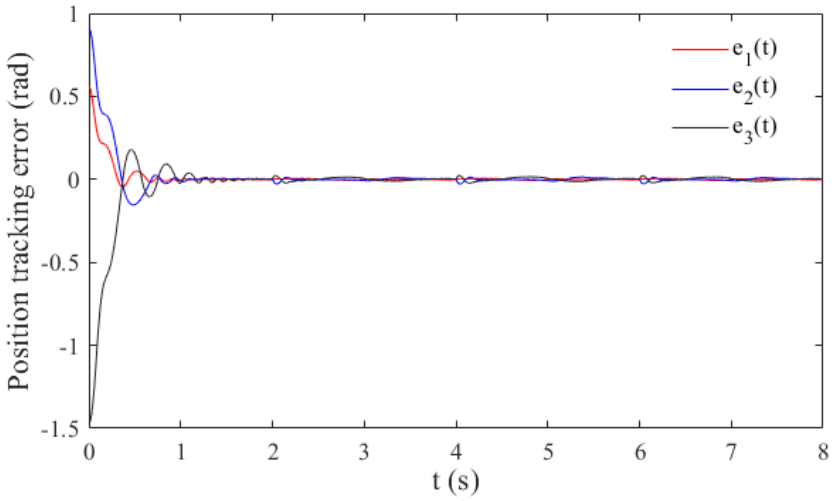

Figure 10: Angular position tracking errors of the first juggler robot.

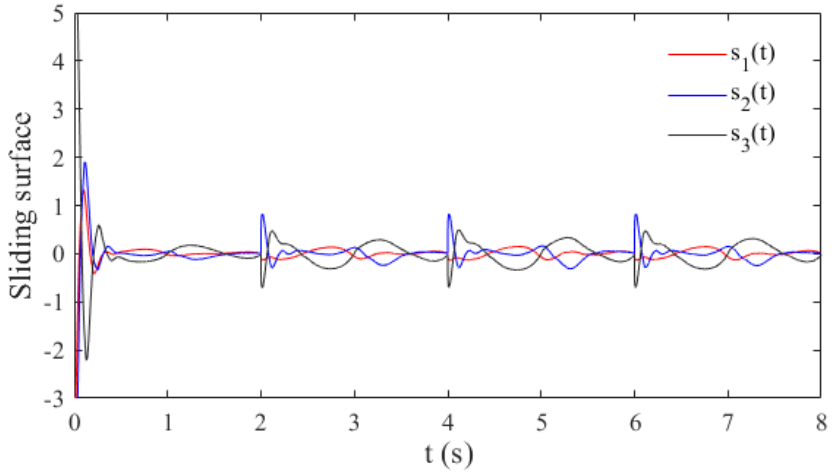

Figure 11: The behaviour of sliding variables.

will inevitably result in increasing the amplitude and chattering of the control efforts and more energy consumption of the system. The control signals are plotted in Fig. 17(a)-(c). The ISMC and FOSMC provide larger control efforts having chattering phenomenons along with impact effects in impact times, which saturation limiters should confine them. Therefore, the necessity of using an actuator limiter is sensible in this example. As shown in these plots, our control approach provides a smooth control signal without the chattering effect. Therefore, it seems that the proposed design is more suitable for real implementation.

To further evaluate the performance of the proposed control scheme another case study is carried out. The maximum saturation limits of the actuators are now set to $\tau_{max} = \begin{bmatrix} 10 & 20 & 20 \end{bmatrix}^T$, while the input delay is increased to $t_d = 2.5 \times 10^{-2}$ s. Then, the control energy (CE) factor of each actuator and the root-mean-square (RMS) tracking errors of the joins are calculated. RMS and CE indicate the tracking error performance and the amount of the control effort, which is proportional to the energy consumption of the juggler robot, respectively. CE for i^{th} actuator is defined as $CE_i = \int_0^{t_f} \tau_i^2(t)\, dt$, where t_f is the final time of the simulation. In Table 1, the results of applying controller (45) with and without using auxiliary system's states (35) and (37) in controller structure are given as Case A and Case B, respectively. These comparative results show that the joints' tracking performances are reduced in Case B, while the

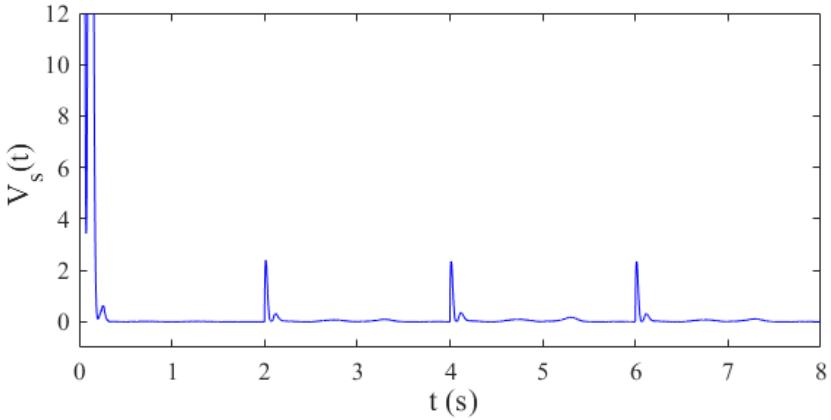

Figure 12: Energy $V_s(t)$.

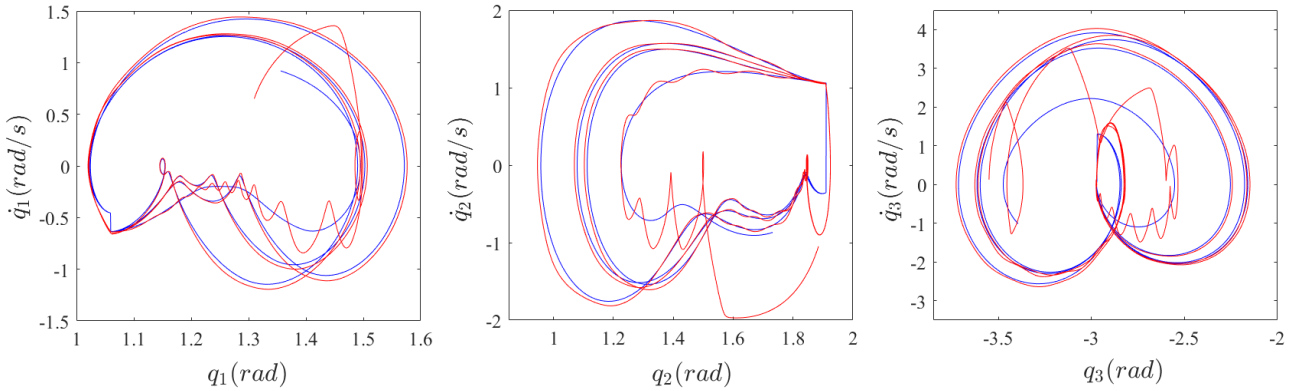

Figure 13: Phase portraits of the desired, blue line, and measured, red line, states of the first juggler robot.

Table 1: Root mean square (RMS) values and control energy (CE) factors for three joints of the first juggler robot. Case A: under controller (45), and Case B: under controller (45) and without using auxiliary system's states (35) and (37) in controller structure.

Controller	Joint i	RMS (rad)	CE $(Nm)^2$
Case A	Joint 1	0.0143	68.1013
	Joint 2	0.0435	196.3930
	Joint 3	0.0783	375.7741
Case B	Joint 1	0.0253	98.0337
	Joint 2	0.0784	286.8629
	Joint 3	0.1336	523.2351

system's energy consumption is increased.

Therefore, our theoretical predictions are validated as the effectiveness of the proposed control scheme.

5. Conclusion

In this paper, an observer-based robust tracking controller design for impulsive hybrid mechanical systems with input delay and actuator saturation has been investigated. A state augmented technique has been employed to deal with the lumped disturbance function, while two novel compensation systems were put forwarded to handle input delays and actuator constraints. A centralized robust fractional-order sliding mode controller was designed using

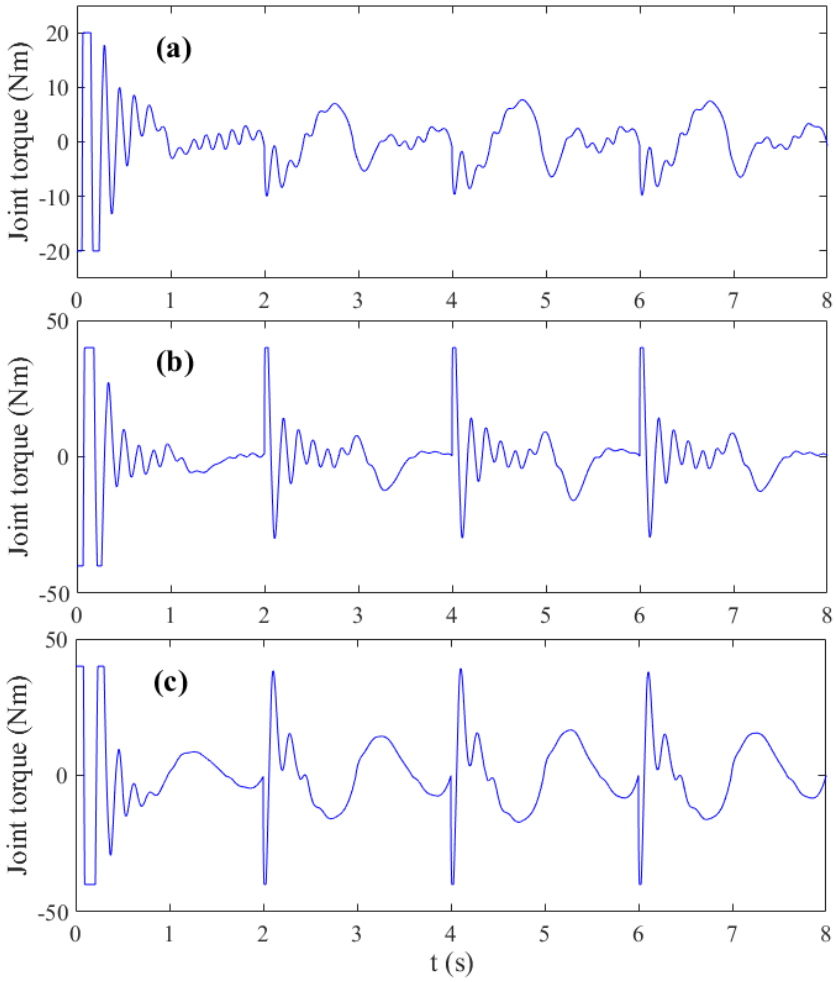

Figure 14: Control efforts of the joints of the first juggler robot: (a) τ_1, (b) τ_2, and (c) τ_3.

these auxiliary systems' states and the extended-state observer's estimation results. It has been proved that the joint position/velocity tracking errors and the observer tracking errors converge to the origin in a finite-time. The efficiency of the proposed theoretical methods was evaluated on a ball-playing juggler robot.

Future studies will be focused on a robust adaptive controller design for hybrid pH systems with unknown time delays in system states, unknown control direction, and under practical constraints on system states and control signal. The theoretical results will then be implemented on real robotic systems such as biped robots and ball juggler robots.

Appendix A

The details of three matrices M_1, C_1, and g_{0_1} for the first juggler robot are as follows:

$$M_1 = \begin{bmatrix} M_{11} & M_{12} & M_{13} \\ M_{21} & M_{22} & M_{23} \\ M_{31} & M_{32} & M_{33} \end{bmatrix}, C_1 = \begin{bmatrix} C_{11} & C_{12} & C_{13} \\ C_{21} & C_{22} & C_{23} \\ C_{31} & C_{32} & C_{33} \end{bmatrix}, \text{and } g_{0_1} = \begin{bmatrix} g_{0_{11}} \\ g_{0_{12}} \\ g_{0_{13}} \end{bmatrix}, \text{where}$$

$$M_{11} = \frac{1}{3}m_1L_1^2 + \frac{1}{3}m_2(3L_1^2 + 3L_1L_2c_2 + L_2^2) + \frac{1}{3}m_3(3L_1^2 + 6L_1L_2c_2 + 3L_1L_3c_{23} + 3L_2^2 + 3L_2L_3c_3 + L_3^2),$$

$$M_{12} = \frac{1}{6}m_3(6L_2^2 + 6L_2L_3c_3 + 6L_1L_2c_2 + 2L_3^2 + 3L_1L_3c_{23}) + \frac{1}{6}m_2L_2(2L_2 + 3L_1c_2),$$

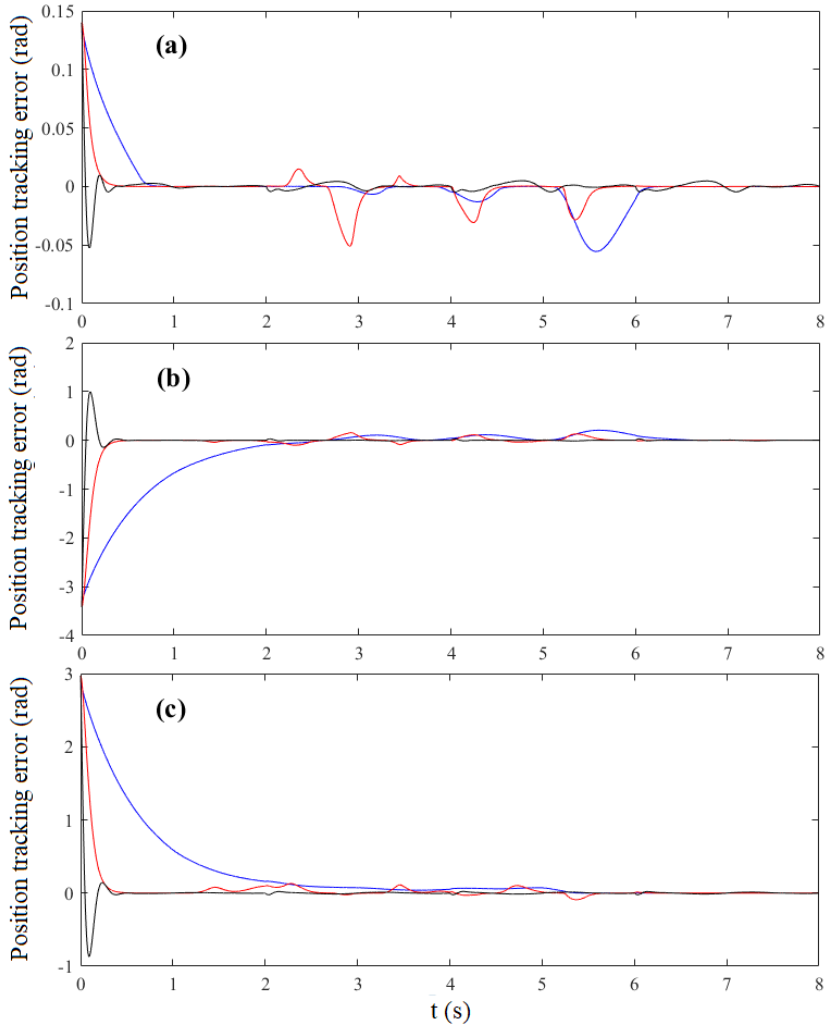

Figure 15: Angular position tracking errors with the proposed controller (black lines), integral sliding mode control [49] (red lines), and fractional-order sliding mode control [52] (blue lines): (a) position tracking error of joint 1, (b) position tracking error of joint 2, and (c) position tracking error of joint 3.

$$
\begin{aligned}
M_{13} &= \frac{1}{6}m_3L_3(2L3 + 3L_1c_{23} + 3L_2c_3),\\
M_{21} &= M_{12},\\
M_{22} &= \frac{1}{3}m_3(3L_2^2 + 3L_2L_3c_3 + L_3^2) + \frac{1}{3}m_2L_2^2,\\
M_{23} &= \frac{1}{6}m_3L_3(2L_3 + 3L_2c_3),\\
M_{31} &= M_{13},\\
M_{32} &= M_{23},\\
M_{33} &= \frac{1}{3}m_3L_3^2,\\
C_{11} &= -\Big(\frac{1}{2}m_3L_1(L_3s_{23} + 2L_2s_2) + \frac{1}{2}m_2L_1L_2s_2\Big)\dot{q}_2 - \frac{1}{2}m_3L_3(L_1s_{23} + L_2s_3)\dot{q}_3,\\
C_{12} &= -\Big(\frac{1}{2}m_3L_1(L_3s_{23}+2L_2s_2)+\frac{1}{2}m_2L_1L_2s_2\Big)\dot{q}_1-\Big(\frac{1}{2}m_3L_1(L_3s_{23}+2L_2s_2)+\frac{1}{2}m_2L_1L_2s_2\Big)\dot{q}_2-\frac{1}{2}m_3L_3(L_1s_{23}+L_2s_3)\dot{q}_3,\\
C_{13} &= -\frac{1}{2}m_3L_3(L_1s_{23} + L_2s_3)\dot{q}_3 - \frac{1}{2}m_3L_3(L_1s_{23} + L_2s_3)\dot{q}_1 - \frac{1}{2}m_3L_3(L_1s_{23} + L_2s_3)\dot{q}_2,
\end{aligned}
$$

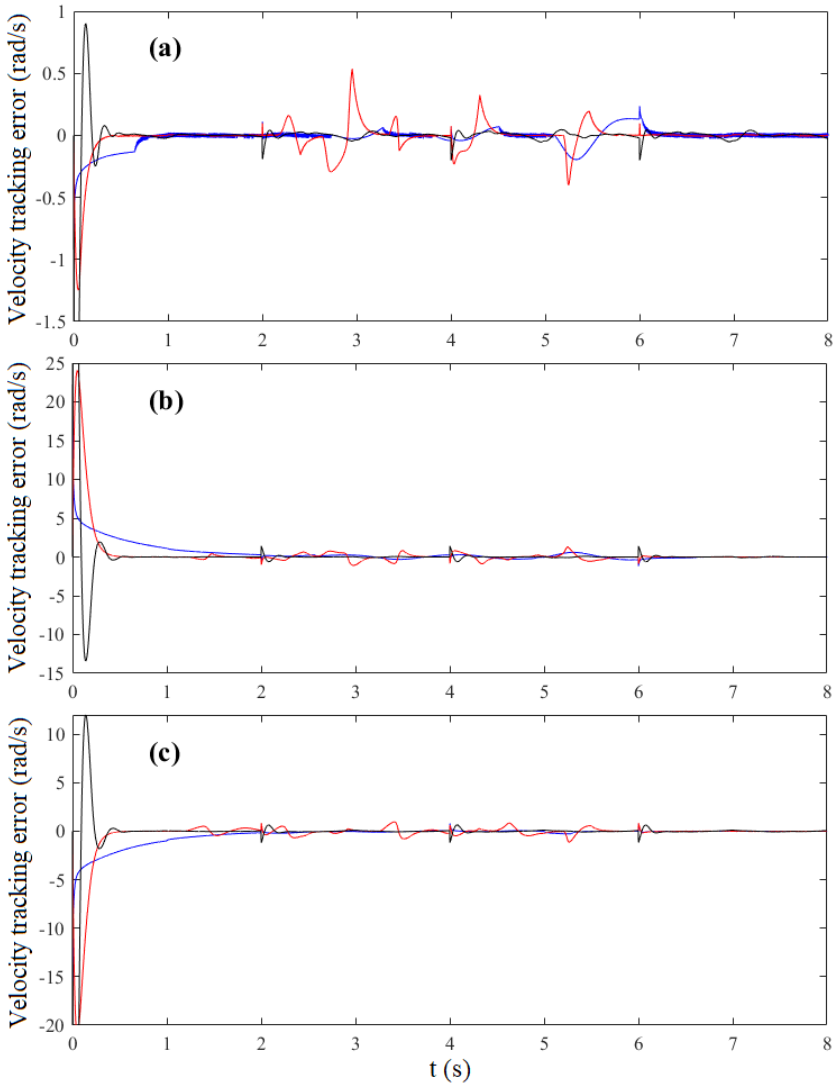

Figure 16: Angular velocity tracking errors with the proposed controller (black lines), integral sliding mode control [49] (red lines), and fractional-order sliding mode control [52] (blue lines): (a) velocity tracking error of joint 1, (b) velocity tracking error of joint 2, and (c) velocity tracking error of joint 3.

$$
\begin{aligned}
C_{21} &= \Big(\frac{1}{2}m_3L_1(L_3s_{23}+2L_2s_2)+\frac{1}{2}m_2L_1L_2s_2\Big)\dot{q}_1-\frac{1}{2}m_3L_2L_3s_3\dot{q}_3,\\
C_{22} &= -\frac{1}{2}m_3L_2L_3s_3\dot{q}_3,\\
C_{23} &= -\frac{1}{2}m_3L_2L_3s_3\Big(\dot{q}_1+\dot{q}_2+\dot{q}_3\Big),\\
C_{31} &= \frac{1}{2}m_3L_3(L_1s_{23}+L_2s_3)\dot{q}_1+\frac{1}{2}m_3L_2L_3s_3\dot{q}_2,\\
C_{32} &= \frac{1}{2}m_3L_2L_3s_3\Big(\dot{q}_1+\dot{q}_2\Big),\\
C_{33} &= 0,\\
g_{0_{11}} &= gm_3(L_1c_1+L_3c_{123}+L_2c_{12})+gm_2(L_1c_1+L_2c_{12})-\frac{1}{2}gm_2L_2c_{12}+\frac{1}{2}gm_1L_1c_1-\frac{1}{2}gm_3L_3c_{123},\\
g_{0_{12}} &= \frac{1}{2}gm_2L_2c_{12}+gm_3\Big(\frac{1}{2}L_3c_{123}+L_2c_{12}\Big),
\end{aligned}
$$

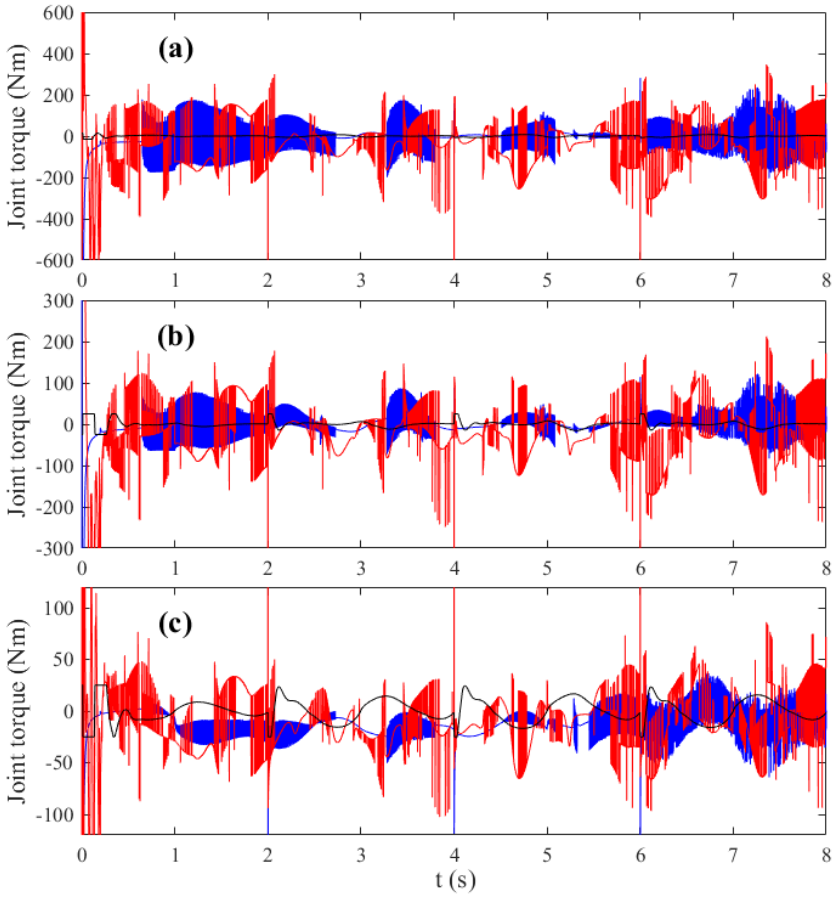

Figure 17: Control efforts with the proposed controller (black lines), integral sliding mode control [49] (red lines), and fractional-order sliding mode control [52] (blue lines): (a) τ_1, (b) τ_2, and (c) τ_3.

$g_{0_{13}} = \frac{1}{2} g m_3 L_3 c_{123}$,

where $c_1 = \cos(q_1)$, $c_2 = \cos(q_2)$, $c_3 = \cos(q_3)$, $s_2 = \sin(q_2)$, $s_3 = \sin(q_3)$, $c_{12} = \cos(q_1 + q_2)$, $c_{23} = \cos(q_2 + q_3)$, $c_{123} = \cos(q_1 + q_2 + q_3)$, and $s_{23} = \sin(q_2 + q_3)$.

Acknowledgment

The research leading to these results has been supported by both the PRINBOT project (in the frame of the PRIN 2017 research program, grant number 20172HHNK5_002) and the WELDON project (in the frame of Programme STAR, financially supported by UniNA and Compagnia di San Paolo). The authors are solely responsible for its content.

References

[1] A. van der Schaft, L2-gain and passivity techniques in nonlinear control, Springer-Verlag, London, 2000.
[2] E. Francoa, A. G. Casanovas, A. Donaire, Energy shaping control with integral action for soft continuum manipulators, Mechanism and Machine Theory 158 (2021) 104250.
[3] B. Fu, S. Li, X. Wang, L. Guo, Output feedback based simultaneous stabilization of two port-controlled Hamiltonian systems with disturbances, Journal of the Franklin Institute 356 (2019) 8154–8166.
[4] Z. Jia, L. Qiao, W. Zhang, Adaptive tracking control of unmanned underwater vehicles with compensation for external perturbations and uncertainties using port-Hamiltonian theory, Ocean Engineering 209 (2020) 107402.

[5] M. Djemai, M. Defoort, Hybrid dynamical systems: Observation and control, Springer-Verlag, London, 2015.
[6] Z. M. Wang, A. Wei, X. Zhao, J. Yang, G. Zong, Stabilisation and H_∞ control for switched port-controlled Hamiltonian systems with unstable modes and actuator saturation, International Journal of Systems Science 51 (1) (2020) 1–19.
[7] X. Yang, D. Peng, X. Lv, X. Li, Recent progress in impulsive control systems, Mathematics and Computers in Simulation 155 (2019) 244–268.
[8] I. Nodozi, M. Rahmani, LMI-based model predictive control for switched nonlinear systems, Journal of Process Control 59 (2017) 49–58.
[9] S. Yang, C. Guo, B. Liu, X. Lin, C. Zhao, Decentralized and autonomous voltage balancing control approach for hybrid multi-terminal ultra-HVDC system, International Journal of Electrical Power and Energy Systems 115 (2020) 105472.
[10] G. X. Zhong, G. H. Yang, Passivity and output feedback passification of switched continuous-time systems with a dwell time constraint, Journal of Process Control 32 (2015) 16–24.
[11] W. Chen, C. Wen, J. Wu, Global exponential/finite-time stability of nonlinear adaptive switching systems with applications in controlling systems with unknown control direction, IEEE Transactions on Automatic Control 63 (2018) 2738–2744.
[12] F. Wu, J. Lian, Stabilization of constrained switched systems via multiple Lyapunov R-functions, Systems and Control Letters 139 (2020) 104686.
[13] M. A. Müller, P. Martius, F. Allgöwer, Model predictive control of switched nonlinear systems under average dwell-time, Journal of Process Control 22 (2012) 1702–1710.
[14] Z. M. Wang, A. Wei, X. Zhang, Stability analysis and control design based on average dwell time approaches for switched nonlinear port-controlled Hamiltonian systems, Journal of the Franklin Institute 365 (6) (2019) 3368–3397.
[15] A. Mattioni, Y. W. aand Hector Ramirez, Y. Gorrec, A. Macchelli, Modelling and control of an IPMC actuated flexible structure: A lumped port Hamiltonian approach, Control Engineering Practice 101 (6) (2020) 104498.
[16] E. Franco, T. Brown, A. Astolfi, F. R. Baena, Adaptive energy shaping control of robotic needle insertion, Mechanism and Machine Theory 155 (2021) 104060.
[17] R. Rashad, F. Califano, S. Stramigioli, Port-Hamiltonian passivity-based control on $se(3)$ of a fully actuated UAV for aerial physical interaction near-hovering, IEEE Robotics and Automation Letters 4 (4) (2019) 4378–4385.
[18] A. van der Schaft, D. Jeltsema, Port-Hamiltonian Systems Theory: An Introductory Overview, Now Foundations and Trends, 2014.
[19] S. Dai, X. Koutsoukos, Safety analysis of integrated adaptive cruise and lane keeping control using multi-modal port-Hamiltonian systems, Nonlinear Analysis: Hybrid Systems 35 (2020) 100816.
[20] H. Gritli, N. Khraief, A. Chemori, S. Belghith, Self-generated limit cycle tracking of the underactuated inertia wheel inverted pendulum under IDA-PBC, Nonlinear Dynamics 89 (2017) 2195–2226.
[21] A. Venkatraman, A. van der Schaft, Full-order observer design for a class of port-Hamiltonian systems, Automatica 46 (2010) 555–561.
[22] B. Fu, Q. Wang, W. He, Nonlinear disturbance observer-based control for a class of port-controlled Hamiltonian disturbed systems, IEEE Access 6 (2018) 50299–50305.
[23] Z. M. Wang, A. Wei, X. Zhao, J. Yang, G. Zong, Stabilisation and H_∞ control for switched port-controlled Hamiltonian systems with unstable modes and actuator saturation, International Journal of Systems Science 51 (1) (2020) 1–19.
[24] F. Ruggiero, V. Lippiello, B. Siciliano, Nonprehensile dynamic manipulation: A survey, IEEE Robotics and Automation Letters 3 (3) (2018) 1711–1718.
[25] D. Serra, F. Ruggiero, V. Lippiello, B. Siciliano, A nonlinear least squares approach for nonprehensile dual-hand robotic ball juggling, IFAC-PapersOnLine 50 (1) (2017) 11485–11490.
[26] O. Koç, G. Maeda, J. Peters, Online optimal trajectory generation for robot table tennis, Robotics and Autonomous Systems 105 (2018) 121–137.
[27] K. Zhang, Z. Cao, J. Liu, Z. Fang, M. Tan, Real-time visual measurement with opponent hitting behavior for table tennis robot, IEEE Transactions on Instrumentation and Measurement 67 (2018) 811–820.
[28] H. Su, Z. Fang, D. Xu, M. Tan, Trajectory prediction of spinning ball based on fuzzy filtering and local modeling for robotic ping–pong player, IEEE Transactions on Instrumentation and Measurement 62 (2013) 2890–2900.
[29] Y. Zhao, Y. Zhang, R. Xiong, J. Wang, Optimal state estimation of spinning ping-pong ball using continuous motion model, IEEE Transactions on Instrumentation and Measurement 64 (2015) 2208–2216.
[30] H. Gritli, S. Belghith, LMI-based synthesis of a robust saturated controller for an underactuated mechanical system subject to motion constraints, European Journal of Control 57 (2021) 179–193.
[31] Y. Wei, G. P. Liu, Composite control for switched impulsive time-delay systems subject to actuator saturation and multiple disturbances, Nonlinear Analysis: Hybrid Systems 35 (2020) 100825.
[32] H. Ye, M. Li, C. Yang, W. Gui, Finite-time stabilization of the double integrator subject to input saturation and input delay, IEEE/CAA Journal of Automatica Sinica 5 (2018) 1017–1024.
[33] X. Lin, W. Zhang, S. Huang, E. Zheng, Finite-time stabilization of input-delay switched systems, Applied Mathematics and Computation 375 (2020) 125062.
[34] L. A. Tuan, Fractional-order fast terminal back-stepping sliding mode control of crawler cranes, Mechanism and Machine Theory 137 (2019) 297–314.
[35] N. Bigdeli, The design of a non-minimal state space fractional-order predictive functional controller for fractional systems of arbitrary order, Journal of Process Control 356 (29) (2015) 45–56.
[36] S. Song, B. Zhang, X. Song, Y. Zhang, Z. Zhang, W. Li, Fractional-order adaptive neuro-fuzzy sliding mode H_∞ control for fuzzy singularly perturbed systems, Journal of the Franklin Institute 356 (10) (2019) 5027–5048.
[37] M. Alinezhad, T. Allahviranloo, On the solution of fuzzy fractional optimal control problems with the Caputo derivative, Information Sciences 421 (2) (2017) 218–236.
[38] Y. Farid, V. J. Majd, A. Ehsani-Seresht, Fractional-order active fault-tolerant force-position controller design for the legged robots using saturated actuator with unknown bias and gain degradation, Mechanical Systems and Signal Processing 104 (2018) 465–486.
[39] X. Yang, C. Yang, C. Yang, T. Peng, Z. Chen, Z. Wu, W. Gui, Transient fault diagnosis for traction control system based on optimal fractional-

order method, ISA Transactions (2020) 317–329.
[40] J. Liu, P. Li, L. Qi, W. Chen, K. Qin, Distributed formation control of double-integrator fractional-order multi-agent systems with relative damping and nonuniform time-delays, Journal of the Franklin Institute 365 (10) (2019) 5122–5150.
[41] W. Znegui, H. Gritli, S. Belghith, Stabilization of the passive walking dynamics of the compass-gait biped robot by developing the analytical expression of the controlled poincaré map, Nonlinear Dynamics 101 (2020) 1061–1091.
[42] F. Turki, H. Gritli, S. Belghith, An LMI-based design of a robust state-feedback control for the master-slave tracking of an impact mechanical oscillator with double-side rigid constraints and subject to bounded-parametric uncertainty, Communications in Nonlinear Science and Numerical Simulation 82 (2020) 105020.
[43] H. Gritli, Robust master-slave synchronization of chaos in a one-sided 1-dof impact mechanical oscillator subject to parametric uncertainties and disturbances, Mechanism and Machine Theory 142 (2019) 103610.
[44] C. Lanczos, The variational principles of mechanics, University of Toronto press, 1952.
[45] Y. Farid, F. Ruggiero, Finite-time disturbance reconstruction and robust fractional-order controller design for hybrid port-Hamiltonian dynamics of biped robots, Robotics and Autonomous Systems 144 (2021) 103836.
[46] Y. Wang, G. Feng, Finite-time stabilization of port-controlled Hamiltonian systems with application to nonlinear affine systems, 2008, pp. 1202–1207.
[47] H. Liu, Y. Shen, X. Zhao, Asynchronous finite-time H_∞ control for switched linear systems via mode-dependent dynamic state-feedback, Nonlinear Analysis: Hybrid Systems 8 (2013) 109–120.
[48] A. A. Kilbas, H. M. Srivastava, J. J. Trujillo, Theory and Application of Fractional Differential Equations, Elsevier, Amsterdam, 2006.
[49] X. Lv, Y. Niu, J. Song, Finite-time boundedness of uncertain Hamiltonian systems via sliding mode control approach, Nonlinear Dynamics 104 (2021) 497–507.
[50] B. Siciliano, L. Sciavicco, L. Villani, G. Oriolo, Robotics —Modelling, Planning and Control, Springer-Verlag, London, 2009.
[51] V. Lippiello, F. Ruggiero, B. Siciliano, 3D monocular robotic ball catching, Robotics and Autonomous Systems 61 (2013) 1615–1625.
[52] M. Tofigh, M. Mahjoob, M. Hanachi, M. Ayati, Fractional sliding mode control for an autonomous two-wheeled vehicle equipped with an innovative gyroscopic actuator, Robotics and Autonomous Systems 140 (4) (2021) 103756.